Biogeosciences Discuss., 4, 4323–4384, 2007
www.biogeosciences-discuss.net/4/4323/2007/

Biogeosciences Discussions

Biogeosciences Discussions is the access reviewed discussion forum of *Biogeosciences*

A dynamic global model for planktonic foraminifera

I. Fraile[1], **M. Schulz**[1,2], **S. Mulitza**[2], **and M. Kucera**[3]

[1]Department of Geosystem modelling, University of Bremen, P.O. Box 330440, 28334 Bremen, Germany
[2]DFG Research Center Ocean Marigins, University of Bremen, P.O. Box 330440, 28334 Bremen, Germany
[3]Institute of Geosciences, Eberhard Karls University of Tübingen, Sigwartstrasse 10, 72076 Tübingen, Germany

Received: 17 October 2007 – Accepted: 17 October 2007 – Published: 26 November 2007

Correspondence to: I. Fraile (igaratza@palmod.uni-bremen.de)

Abstract

Seasonal changes in the flux of planktonic foraminifera have to be understood to interpret corresponding proxy-based reconstructions. To study the seasonal cycle of planktonic foraminifera species we developed a numerical model of species concentration (PLAFOM). This model is forced with a global hydrographic dataset (e.g. temperature, mixed layer depth) and with biological information taken from an ecosystem model (e.g. "food type", zooplankton abundance) to predict monthly concentrations of the most common planktonic foraminifera species used for proxies: *N. pachyderma* (sinistral and dextral varieties), *G. bulloides*, *G. ruber* (white variety) and *G. sacculifer*. The sensitivity of each species with respect to temperature (optimal temperature and range of tolerance) is derived from sediment-trap studies.

Overall, the spatial distribution patterns of most of the species are comparable to core-top data. *N. pachyderma* (sin.) is limited to polar regions, *N. pachyderma* (dex.) and *G. bulloides* are the most common species in high productivity zones like upwelling areas, while *G. ruber* and *G. sacculifer* are more abundant in tropical and subtropical oligotrophic waters. Modeled seasonal variation match well with sediment-trap records in most of the locations for *N. pachyderma* (sin), *N. pachyderma* (dex.) and *G. bulloides*. *G. ruber* and *G. sacculifer* show, in general, lower concentrations and less seasonal variability in all sites. The lower variability is reflected in the model output, but the small scale variations are not reproduced by the model in several locations. Due to the fact that the model is forced by climatological data, it can not capture interannual variations. The sensitivity experiments we carried out show that, inside the temperature tolerance range, food availability is the main parameter which controls the abundance of some species.

The here presented model represents a powerful tool to explore the response of planktonic foraminifera to different boundary conditions, and to quantify the seasonal bias in foraminifera-based proxy records.

1 Introduction

Planktonic foraminifera are widely used for paleoceanographic reconstructions. They constitute a minor percentage of total zooplankton, but the deposition of their shells on the ocean floor contributes substantially to sediments. Individual species of planktonic foraminifera are essentially distributed geographically as well as vertically in the water column, according to their requirements for physiology, feeding and reproduction within specific temperature ranges (e.g., Bé and Hamilton, 1967; Bé and Tolderlund, 1971). Shells of planktonic foraminifera extracted from marine sediments serve as an archive of chemical and physical signals that can be used to quantify past environmental conditions, such as sea-water temperature (e.g., Pflauman et al., 1996; Malmgren et al., 2001), stratification of the thermocline (e.g., Mulitza et al., 1997), atmospheric CO_2 concentration (Pearson and Palmer, 2000) and biological productivity (Kiefer, 1998). Past sea-surface temperatures can be estimated by either quantifying differences between modern and fossil species assemblages (e.g., CLIMAP, 1976; Pflauman et al., 1996; Malmgren et al., 2001); or by analyzing the isotopic or trace-element composition of calcite in the shell (e.g., Rohling and Cooke, 1999; Lea, 1999). In general, all estimation procedures are based on a correlation between modern conditions and assemblage composition or shell chemistry. This correlation is applied for the interpretation of the fossil assemblages by statistical techniques of varying complexity to yield an estimation of, e.g., past water temperatures (see, for example, Malmgren et al., 2001).

Seasonal changes in the flux of planktonic foraminifera are strongly influenced by environmental factors, such as sea-surface temperature, the structure of the water column, and the food supply (e.g., Bijma et al., 1990; Ortiz et al., 1995; Watkins et al., 1996; Watkins and Mix, 1998; Eguchi et al., 1999; Schnack-Schiel et al., 2001; King and Howard, 2003a; Morey et al., 2005; Žarić et al., 2005). The seasonality of foraminiferal production is an important factor which has to be taken into account in paleoceanographic interpretations (e.g., Deuser and Ross, 1989; Wefer, 1989; Mulitza

et al., 1998; Ganssen and Kroon, 2000; King and Howard, 2001; Pflauman et al., 2003; Waelbroeck et al., 2005; Simstich, 1999). Any past change in the timing of the seasonal maximum of foraminiferal flux may lead to a bias in estimated paleotemperature. This bias arises because the sedimentary record reflects the convolution of the total foraminiferal flux and temperature. Moreover, this differences in seasonality make the comparison of reconstructed temperatures based on assemblages of planktonic foraminifera with those derived by other sea-surface temperature proxies difficult. For example, Niebler et al. (2003) suggested, that discrepancies in temperature reconstructions applying foraminifera- versus alkenone-based proxies might be due to different ecological and thus seasonal preferences of the proxy producers. Climate change could induce variations in the seasonal succession of the planktonic foraminifera and this variation needs to be quantified to understand corresponding proxy-based reconstructions.

To study the seasonal variations of planktonic foraminifera species we have developed a numerical model for planktonic foraminifera at species level. Previously, Žarić et al. (2006) developed an empirical model based on hydrographic and productivity data. In contrast to the model of Žarić et al. (2006), we present a dynamic model for simulating the growth rate of the foraminifera population. This study shows model predictions for spatial and temporal distribution patterns of the five most important modern planktonic foraminifera used as proxies. We also show the comparison of the model output with observations from surface sediments and sediment traps.

2 Model setup

The geographical distribution of each species and its population density depends on biotic (e.g. food, symbionts) and abiotic factors (e.g. light, temperature). To supply the foraminifera model with ecological information it was coupled to an ecosystem model.

2.1 Ecosystem model

The marine ecosystem model used here (Moore et al., 2002a) is configured for the global mixed-layer of the ocean. It predicts the distribution of zooplankton, diatoms, small phytoplankton (which implicitly includes coccolithophores) and diazotrophs, carries sinking and non-sinking detrital pools, and nitrate, ammonium, phosphate, iron and silicate as nutrients.

The ecosystem model is driven by hydrographic data that is derived from an ocean circulation model and from climatologies. The forcing data include the local processes of turbulent mixing, vertical velocity at the base of the mixed layer, and seasonal mixed-layer entrainment/detrainment. Horizontal advection is not included; thus there is no lateral exchange. For the implementation, all vertical structure is ignored using the mean values of the surface mixed-layer.

Previously, this two-dimensional model has been validated against a diverse set of field observations from several JGOFS (Joint Global Ocean Flux Study) and historical time series locations (Moore et al., 2002a), satellite observations, and global nutrient climatologies (Moore et al., 2002b). The full list of model terms, parametrizations, equations and behaviour in the global domain is described in detail in Moore et al. (2002a,b).

2.2 PLAFOM

The planktonic foraminifera model determines the distribution of the following 5 species: *Neogloboquadrina pachyderma* (sinistral and dextral coiling varieties), *Globigerina bulloides*, *Globigerinoides ruber* (white variety) and *Globigerinoides sacculifer*. These species have often been considered to be sensitive to sea-surface temperature, and therefore their assemblage can be used to estimate past sea-surface temperatures by means of transfer functions.

Each species has a different food preference, and therefore a different maximum prey-dependent growth rate. In general, spinose species prefer animal prey such as

copepods, pteropods, and ostracods (Caron and Bé, 1984; Spindler et al., 1984; Hemleben et al., 1985, 1989; Arnold and Parker, 1999). Non-spinose species are largely herbivorous, although in some specimens muscle tissue has been found in food vacuoles (Anderson et al., 1979). On a seasonal scale, food is assumed to be the predominant factor affecting the distribution of planktonic foraminifera. Planktonic foraminifers appear to respond to the redistribution of nutrients and phytoplankton very quickly, increasing the number of individuals within several days (Schiebel et al., 1995). Information about food availability is obtained from the ecosystem model. In the model, the food sources may be either zooplankton, small phytoplankton, diatoms or organic detritus.

For each species the change in foraminifera concentration, expressed as biomass [mmolC/m^3], is calculated by the following equation:

$$\frac{dF}{dt} = (GGE \cdot \sum \text{grazing}_C) - \text{mortality} \quad (1)$$

where F is the foraminifera carbon concentration, GGE (gross growth efficiency) is the portion of grazed matter that is incorporated into foraminifera biomass, which we assume to be constant regardless of the food source (C). The food sources are diatoms (D), small phytoplankton (SP), zooplankton (Z) or detritus (DR). Each species of foraminifera has a different food preference and therefore this is represented using different grazing proportions. The food supply predicted by the ecosystem model is calculated with reference to carbon weight, the same units as for the foraminifera in the model.

2.2.1 Grazing in PLAFOM

The growth rates are determined by available food using a modified form of Michaelis-Menton kinetics (Eq. 2),

$$\sum \text{grazing}_C = \sum p \cdot \left[G_{\max} \cdot \alpha \cdot F \cdot \left(\frac{C}{(C+g)} \right) \right] \quad (2)$$

where G_{max} is the maximum growth rate, g is the half saturation constant for grazing, α is the relative abundance in relation to temperature, C represents the concentration of each type of food (diatoms, small phytoplankton, zooplankton or detritus), and p is the preference for this food. The values and units of all parameters are summarized in Table 1. The food requirement varies for the different foraminifera species. Many species of planktonic foraminifera consume a wide variety of zooplankton and phytoplankton prey, and they are capable of a reasonably flexible adaptation to varying trophic regimes. The food of *N. pachyderma* (sinistral and dextral varieties) comprises, almost exclusively, of phytoplankton, commonly diatoms (Hemleben et al., 1989). *G. bulloides* presents biological characteristics that place it on the borderline between spinose and non-spinose species; while most spinose species possess algal symbionts *G. bulloides* does not (Hemleben et al., 1989; Murray, 1991). *G. ruber* and *G. sacculifer* are both spinose species hosting dinoflagellate endosymbionts. They feed mostly on zooplankton, although *G. ruber* has lower zooplankton dependence than other spinose species (Hemleben et al., 1989). Culture experiments of *G. sacculifer* confirm that it depends on zooplankton food (Bé et al., 1981). It is adapted to low productivity areas (mainly the centers of the oceanic gyres), perhaps because it obtains nutrition from its symbionts (Watkins et al., 1996); but the seasonal maximum abundance occurs when the productivity in these regions is maximal. To include this contradictory information for the parametrization of *G. ruber* and *G. sacculifer* we use maximum nutrient and chlorophyll concentration as a separate input variable to monthly nutrient and chlorophyll data. Maximum growth rates for the foraminifera (G_{max}) varies with the food source. Since zooplankton carbon concentration is most of the time much lower than phytoplankton carbon concentration, when zooplankton is the food source G_{max} is set higher than when diatoms, small phytoplankton or detritus are the food source. Thus, under typical food availability conditions, carnivore species can growth as fast as herbivore species.

As a result of the general observations that the most marked planktonic foraminifera distribution patterns are latitudinal, we focused on the influence of the temperature

more than in any other physical variable. The experimental work of Bijma et al. (1990) shows evidence for direct control of temperature over vital processes. They showed a correlation between in vitro temperature tolerance limits and the known natural limits of the experimental species. The tolerance limits of most species, however, are not sharply defined. Instead, departure from optimal conditions causes a gradual reduction of vital processes (Arnold and Parker, 1999). Žarić et al. (2005, 2006) compiled a planktonic foraminiferal flux dataset from time-series sediment-trap observations from 42 sites across the world ocean, and analyzed species sensitivity to temperature relating fluxes and relative abundances of seven species to sea-surface temperature. Based on this work, we approximate the temperature relation to a normal distribution. Therefore each species exhibits an optimal SST and an SST tolerance range. The growth rate is limited by temperature through the parameter α (Eq. 3). The relationship with temperature assumes that the foraminifera concentration at any site is normally distributed, with an optimum temperature where the relative abundance is highest. Away from this optimum temperature the relative abundance decreases until a critical temperature beyond which the species does not occur. This pattern, with a central peak and symmetrical tails, can be approximated by Gaussian distribution (Eq. 3). The value of α varies between 0 (out of limit of tolerance) and 1 (optimal temperature).

$$\alpha = \left[n \cdot \exp\left[-0.5 \cdot \left(\frac{(T_s - T_{\text{opt}})}{\sigma} \right)^2 \right] \right]^{\left(\frac{1}{k}\right)} \tag{3}$$

Here, n is a parameter to scale the values of α between 0 and 1. The normal distribution is characterized by two parameters: the optimal temperature, T_{opt}; and some variability expressed as standard deviation, σ, which represents the SST (T_s) tolerance range of a give species. Species with small σ are more sensitive to temperature. 1σ around T_{opt} accounts for the temperature where about the 68% of the population is living. The values of all parameters for each species are summarized in Table 2. Of the five species *G. ruber* (white) and *G. sacculifer* (both tropical species), together with

N. pachyderma (sin.) exhibit the narrowest SST tolerance range. *N. pachyderma* (sin.) is absent at SSTs above 23.7°C (Žarić et al., 2005). *N. pachyderma* (sin.) is a polar species and survives even within the annual sea ice (Antartic), where it feeds on diatoms (Dieckman et al., 1991; Spindler, 1996). *N. pachyderma* (dex.) and *G. bulloides* are present almost throughout the whole oceanic SST range; however, *N. pachyderma* (dex.) exhibits a clear preference for mid-temperatures. For *G. bulloides* temperature does not seem to be a controlling factor. It has the second largest temperature tolerance, after *N. pachyderma* (dex.), and does not show a unimodal distribution when flux is ploted versus temperature (Žarić et al., 2005). *G. bulloides* comprises at least six different genetic types and as a result exhibits a polymodal distribution pattern (Darling et al., 1999, 2000, 2003; Stewart et al., 2001; Kucera and Darling, 2002). Žarić et al. (2005) showed in their study that in the tropical Indian Ocean *G. bulloides* is present at higher temperatures than in the Atlantic and Pacific Ocean. In this region highest abundances of *G. bulloides* occur at SSTs at which Atlantic as well as Pacific samples show reduced fluxes. Since our study is applied at a global scale, temperature calibration is based on the preferred temperatures of *G. bulloides* in the Pacific and Atlantic Ocean; excluding the samples of the North Indian Ocean. Instead, we modified the normal distribution for *N. pachyderma* (dex.) and *G. bulloides* to accept wider limits under high food availability through the parameter k.

2.2.2 Mortality

The mortality equation comprises of three terms representing losses due to respiration, predation by higher trophic levels and competition (Eqs. 4–8).

Since our model does not include lateral advection, a minimum threshold is needed to preserve the foraminifera population over the winter at high latitudes or during periods with insufficient food supply in regions with high seasonal variability. We set the minimum foraminifera biomass at 0.01 mmolC/m^3. When the populations reach this

minimum level the mortality term is set to zero (Eq. 6).

$$\text{mortality} = \text{predation} + \text{respiration} + \text{competition} \tag{4}$$

$$\text{predation} = pl \cdot \exp\left(-b \cdot \left[\frac{1}{T_s} - \frac{1}{T_m}\right]\right) \cdot F_p^2 \tag{5}$$

where

$$F_p = \max((F - 0.01), 0) \tag{6}$$

$$\text{respiration} = rl \cdot F_p \tag{7}$$

$$\text{competition} = \sum \left[F_p \cdot \frac{cl_{ij} \cdot F_i \cdot d}{F_i \cdot d + 0.1}\right] \tag{8}$$

Predators specialized on planktonic foraminifers are not known, therefore the mortality equation does not explicitly depend upon predator abundance. To represent predation we choose a quadratic form dependent on foraminifera biomass itself (Eq. 5). Although not specifically modeled, this may be interpreted either as cannibalism or as predation by a higher trophic level not being explicitly modeled (Steele and Henderson, 1992; Edwards and Yool, 2000). The variable pl represents the quadratic mortality-rate coefficient, which is used to scale mortality to grazing. From a bioenergetic perspective predation is also temperature dependent. Food consumption rates typically increase with increasing temperature; therefore higher trophic levels will exert more predation pressure with increasing temperature (M. Peck, personal communication). b is the parameter used to scale the temperature function between 0 and 1. Note that T_s represents the absolute SST, and the maximum SST (T_m) assumed in the model corresponds to 303.15 K (30°C). The respiration loss is a linear term of 6% per day (rl), the same value as assumed by Moore et al. (2002a) for zooplankton.

Competition occurs between different species of foraminifera inhabiting the same regions. cl_{ij} represents the maximum competition pressure of the species i upon the

species j (varying from 0 to 1), and d is the e-folding constant, which controls the steepness of the Michaelis-Menton equation.

2.3 Standard model experiment: grid, forcing and boundary conditions

The foraminifera model is run for the global surface ocean, with a longitudinal resolution of 3.6°, a varying latitudinal resolution (between 1–2°, with higher resolution near the equator), and a temporal resolution of one month. This corresponds to the resolution of the underlying ecosystem model (Moore et al., 2002a,b) and to the underlying ocean model (Gent et al., 1998). Lateral advection is not included, therefore there is no connection between the gridpoints.

We used the same forcing as Moore et al. (2002a). Mixed-layer temperatures are from World Ocean Atlas 1998 (Levitus, 1982) modified for the model's grid (NODC-WOA98 data provided by the NOAA/OAR/ESRL PSD, Boulder, Colorado, USA, from the web site at http://www.cdc.noaa.gov/), surface shortwave radiation from the ISCCP cloud-cover-corrected dataset (Bishop and Rossow, 1991; Rossow and Schiffer, 1991), mixed-layer depth is based on the density criterion (Monterey and Levitus, 1997). The minimum mixed-layer depth is set at 25 m. The vertical velocity at the base of mixed layer is derived from the NCAR-3D ocean model. Since lateral advection is not explicitly included these data are smoothed and modified to account for the effect of lateral advection in upwelling areas. The turbulent exchange rate at the base of the mixed layer is set at a constant value of 0.15 m/day. Sea-ice coverage was obtained from the EOSDIS NSIDC satellite data (Cavalieri et al., 1990). Atmospheric iron flux was obtained from the dust deposition model study of Tegen and Fung (1994, 1995). More details about the forcing can be obtained from Moore et al. (2002a).

Bottom boundary conditions are the same as for the zooplankton component of the ecosystem model. For all foraminifera species we assumed a uniform distribution inside the mixed layer, whereas below the mixed layer the concentration was calculated as a function of the surface concentration and the mixed-layer depth. When the mixed-layer is shallow (a minimum of 25 m) the concentration below the mixed-layer will be

the 75% of the surface concentration. With the increasing of the mixed-layer depth, the concentration below it decreases linearly, until reaching the value 0 at a mixed layer depth of 100 m. This is a realistic limit, as the maximum production of the species in questions occurs within this depth range (Bé, 1977; Duplessy et al., 1981; Murray, 1991; Watkins and Mix, 1998).

2.4 Comparison to core-top data

We used the Brown University Foraminiferal Database (Prell et al., 1999) to compare our model results with sedimentary faunal assemblages. This database contains core-top planktonic foraminifera counts from 1264 cores throughout the world ocean. We extended this database with the dataset by Pflauman et al. (1996), which contains planktonic foraminifera counts for 738 surface samples from the North and South Atlantic; and with another 57 core-top samples from the eastern Indian Ocean (Martinez et al., 1998). For comparison with the model output the faunal data were transformed to relative abundances of the 5 foraminifera species simulated with our model. Another adaptation of this dataset has been done to take into account the size differences of each species. Then, the number of individuals were transformed to biomass (mgC/m^3). For this transformation, we calculated the volume occupied by the cytoplasm approximating the shape of all the species to a sphere and assuming that all the volume is occupied by the cytoplasm. For the mean size of each species we used sediment-trap data from Peeters et al. (1999). We assumed the carbon content of the cytoplasm is the same in all species, $0.089\,pgC/\mu m^3$ (Michaels et al., 1995).

To asses the deviation between observed and modeled species distribution we calculated the root mean squared error (RMSE). For this, each core-top data was compared to the nearest model grid point. No averaging was applied to the core-top data. This is justified because the observational data base is identical for all species and our interest is only in comparing model performance for the five species. For the inter-hemispheric comparison coretop data were regridded to the model grid; and the average value was calculated between core-top data corresponding to the same grid point.

2.5 Comparison to sediment-trap data

Several sediment-trap studies were used to compare measured and modeled foraminiferal fluxes. We used the global database compiled originally by Žarić et al. (2005) and extended later in Žarić et al. (2006). This database contains planktonic foraminiferal fluxes calculated from various sediment-trap investigations all over the world. To compare the modeled and observed annual distribution of the different planktonic foraminifera species we used the datasets with a minimum collecting period of one year and with a maximum resolution of one month. We extended the database of Žarić et al. (2005, 2006) by adding trap data from the Northwest Pacific (Motoyoshi and Makoto, 2005; Xu et al., 2005), Bering Sea (Asahi and Takahashi, 2007), South China Sea (Tian et al., 2005) and from the Arabian Sea (Schulz et al., 2002). Table 2 summarizes locations, details and references of the sediment-trap studies used in this study. Figure 1 ilustrates locations of the sediment-trap stations.

Sediment traps show a high temporal resolution and record the flux continuously over several months or years. Because of the sinking speed of foraminiferal shells (150–1300 m/day depending on their weight and size, Takahashi and Be, 1984), the sediment-trap samples are not significantly affected by dissolution, lateral advection or bioturbation and therefore can be directly related to modern surface hydrography (e.g., Tedesco and Thunell, 2003; Marchant et al., 2004; Mohiuddin et al., 2004; Žarić et al., 2005). However, due to the short duration of the collecting periods (most of the available data are for several month or few years) those data may represent local processes of a particular year rather than a long term mean.

3 Results

3.1 Spatial distribution patterns

Modeled global distribution patterns of the five foraminifera species are compared to core-top data (Fig. 2–6). The results shown here correspond to the relative abundances (in biomass) of individual species considering only the five species included in the model. The global output of *N. pachyderma* (sin.) shows the lowest mean squared error, around 10%, while for the rest of the species it varied between 20% and 25%.

N. pachyderma (sin.) is a cold-water species. Previous work showed that it can survive and grow within Antartic sea ice, where diatom concentration is higher than in the water column (Dieckman et al., 1991; Spindler, 1996; Schnack-Schiel et al., 2001). Core-top as well as modeled assemblages show the highest relative abundances (up to 100%) in polar waters (Fig. 2).

N. pachyderma (dex.) is typical of subpolar to transitional water masses. In the sediment surface samples *N. pachyderma* (dex.) shows a very high relative abundance in North Atlantic, in the Benguella upwelling system, parts of the Southern Ocean and in the equatorial Pacific upwelling. It is also present in lower abundance in the upwelling systems of northwest of Africa. The model output shows very high concentrations in the Peru-Chile current and the eastern boundary upwelling systems, as well as south of Island, and moderate abundances at mid latitudes (Fig. 3).

Like *N. pachyderma* (dex.), *G. bulloides* is typical of subpolar (Bé, 1977; Bradshaw, 1959) and transitional water masses (Tolderlund and Be, 1971), and is also found in upwelling areas (Duplessy et al., 1981; Hemleben et al., 1989; Thunell and Reynolds, 1984). Temperature does not seem to be a controlling factor in the distribution of this species, althought the exact relationships between environmental parameters and distribution in *G. bulloides* may be masked by the fact that this species group comprises several distinct genotypes (Darling et al., 1999, 2000, 2003; Stewart et al., 2001; Kucera and Darling, 2002). Generally, the abundance of *G. bulloides* is related to high productivity areas (Prell and Curry, 1981; Bé et al., 1985; Hemleben et al., 1989; Gi-

raudeau, 1993; Watkins and Mix, 1998; Žarić et al., 2005). *G. bulloides* shows a high relative abundance in the surface sediment samples of the North Atlantic Ocean, the upwelling systems of northwest of Africa and Benguela, the Southern Ocean, the North Indian Ocean and with to a lesser extent the upwelling region of Baja California. The model results show high concentrations of *G. bulloides* in the subpolar waters of both hemispheres, in the eastern boundary currents of the southern hemisphere and in some locations of the Arabian Sea (Fig. 4).

G. ruber exhibits two varieties; a pink and a white form. The pink variety is limited to the Atlantic Ocean, therefore we have only modeled the white variety. *G. ruber* (white) is a spinose species generally found in tropical to subtropical water masses. It hosts dinoflagellate endosymbionts (Hemleben et al., 1989), and is omnivorous. These characteristics of bearing spines, utilization of zooplankton prey and symbiotic association are typical of foraminifers adapted to oligotrophic waters. Watkins et al. (1996) suggested that the adaptation to oligotrophic waters could be because they obtain nutrition from their symbionts. The seafloor record shows a high relative abundance in the central North and South Atlantic as well as the South Pacific and a less pronounced relative abundance in the South Indian Ocean up to 40° S. The model output shows high relative abundances in tropical and subtropical waters of the Atlantic, Pacific and Indian Oceans, while it is absent, or in very low relative abundances, in the upwelling areas (Fig. 5).

G. sacculifer shows a clear preference for the upper temperature band and is absent at low temperatures (Žarić et al., 2005). Core-top data show it is limited to tropical waters and reflect its narrow temperature tolerance (Fig. 6). The relative abundance is lower compared to the other four species considered in the model. The highest abundances observed in surface sediments appears in the equatorial Pacific and central Indian Ocean. It has very low concentrations in most of the core-top data of the Arabian Sea. The annual distribution pattern reflected in the model is limited to tropical waters, with very high concentrations in the equatorial Pacific. It is absent in eastern upwelling systems as well as in the upwelling of the Arabian Sea.

3.2 Temporal distribution patterns

We used several sediment-trap datasets to assess the modeled seasonal variations in foraminifera abundance. Table 2 summarizes all the datasets we used for the validation of the model. Figures 7–11 show examples of the comparison between the model output and the sediment-trap data. Note that the units we compare are different; the sediment-trap data give fluxes based on individual shells [ind. m^{-2} day^{-1}] whereas the model provides concentrations [mmolC/m^3]. However, we assume that the flux through the water column is proportional to the surface concentration. The measured standing stocks are biased due to the sieve size used in the sediment-traps (125 μm or 150 μm). Most of the shells of foraminifera in juvenile stage are not included in this size fraction. Nevertheless, the objective of our study is to detect relative changes in the seasonal distribution, therefore the absolute values are not very important. In most of the cases the interannual variability is very high, for example in the Wedell Sea where the annual ice expansion plays an important role in the spring bloom, or in upwelling areas, where the intensification of the upwelling and the entrainment of nutrients is related to the wind intensity. It should be noted that the model is forced with climatologies (i.e., long term mean), and therefore is unable to reproduce interannual variabilities.

Figure 7 show examples of *N. pachyderma* (sin.) in northern North Atlantic (a), Northwest Pacific (b) and Wedell Sea (c). In all of these locations the interannual variability is very high, but the timing of the signal matches well between observed and predicted data.

Figure 8 represents results for *N. pachyderma* (dex.) in order to compare sediment-traps from northern North Atlantic (a), Northwest Pacific (b), Walvis Ridge in South Atlantic (c) and Subantartic Zone (d). The data from the northern North Atlantic (upper figure), even with high interannual variability, show a clear increase in *N. pachyderma* (dex.) flux during the summer months. The seasonal pattern of predicted concentrations match fairly well with the trap record. In the Northwest Pacific the sediment-trap data does not show a clear seasonal pattern, but relatively high fluxes are observed

during the late summer and late autumn. Since our time series reflects the variation during a single year this pattern can not be confirmed as a typical pattern for this region. Nevertheless, the model output does match quite well with this pattern. The trap from the Walvis Ridge does not show a clear seasonal pattern during the first year of the sampling (1989). However, during the last two years there is an increase in the population during autumn (from September to December). Although the model output shows a less abrupt situation, it reflects the general two year trend. The last example demonstrates the situation in the Subantartic Zone. Trap data show an increase of the *N. pachyderma* (dex.) population during the austral summer of the years 1997 and 1998. As we expected from the sediment-trap data, the model results show the highest concentrations during the austral summer.

In Fig. 9 we show examples for *G. bulloides* in Northwest and Southeast Atlantic and in Northwest Pacific. The upper figure represents an annual cycle in the Peru-Chile current (30.01° S 73.18° W). The sediment-trap data shows a clear peak during the summer, between the end of December and January. The model, on the other hand, predicts an annual cycle with a double peak; one at the beginning of summer, matching with sediment-trap data; and a second one during the autumn (may and june) not reflected in the trap data. sediment-trap data from Japan Trench, in the Kuroshio current system domain (34.16° N 141.98° E), shows the highest fluxes during the spring (April–May) for two consecutive years. At this location, the model output acts in accordance with observational data. Figure 9c represents another station north of the Kuroshio current, in the Northwest Pacific. The model predicts in this case an annual cycle with two peaks, a small one during the winter (December–January) and the main peak during early summer (May–June). The sediment-trap data shows quite an irregular pattern, but in both sampled years (1997/1998 and 1998/1999) there is an increased flux during winter months, matching with the small peak predicted by the model. During the second sampling year, in 1999, we can observe a second peak in the summer, which was absent in the previous year. The last time series (Fig. 9d) represents the Walvis Ridge, located close to the Benguela upwelling, in the coastal-

open-ocean mixing zone, where we have a three year record of sediment-trap data. It shows a strong seasonality, with a bimodal flux pattern with the maxima occurring in the austral spring and the second peak in fall. The model successfully predicted the bimodal pattern, with the main bloom ocurring in spring.

Seasonal variations of the flux of *G. ruber* (white) are shown in Fig. 10. The upper figure corresponds to the sediment-trap record at station Cape Blanc (21.15° N 20.69° W), northwest of Africa, for a sampling period of approximately 4 years. The first three years were characterized a maximum in *G. ruber* flux during fall. During fall of 1991, however, the peak was absent or delayed. The timing of the model output is in agreement with the data, with high concentrations from summer to winter and low concentrations in spring. The data recorded by the trap located at the western equatorial Atlantic does not show a clear pattern. During the first year of the sampling period it appears to have a bimodal pattern, with high fluxes in the austral summer and winter. During the second year of the sampling period, however, this winter bloom was missing, showing a single maximum in summer. At this site, the model predicts a unimodal pattern with highest fluxes in September–October. In the Bay of Bengal, both model output and trap data show less variability than the other sites. At the Northwest Pacific, South of Japan, sediment-trap data revealed an irregular pattern. However, the data shows overall low flux from December to April with a high peak in June–July. The model predicts high concentrations from November to July with a decrease during the summer months (July–September).

G. sacculifer shows low fluxes in all sediment-trap data used for model validation. In Fig. 11 we present some comparisons of model output and experimental data. In the rest of the stations the model predicts very low concentrations. When the model reaches the threshold value, setted as the minimum population size (0.01 mmolC/m^3), the hydrographic component of the model starts to dominate over the population dynamic itself. Therefore, in most of the locations the comparison is not viable. The upper two panels (a and b in Fig. 11) represent two stations in the northern Indian Ocean, located on a north-south transect of Bay of Bengal. In the northern trap both

the data and the model output show little variability throughout the year. The central trap shows a prominent increase of foraminiferal flux in July. The model prediction is in good agreement with the data in both cases, showing less variability in the northern site and increases of the *G. sacculifer* population during summer in the central site. In the western equatorial Atlantic (northern Brasil Basin) the fluxes were low during the entire sampling period, with maximum values in December and June. The model output does not match the data, with maximum concentrations during April–May and minimum during fall. The last example comes from the central Arabian Sea. In this site, the model predicts concentrations below the threshold value. At such low concentrations, the model is unable to reproduce variations due to the population dynamics component. Therefore, for a better comparison we choose adjacent locations. The trap data shows a bimodal pattern, with a prominent increase increase of flux during the both monsoons (June–August and November–April). Instead of that, the model simulates high concentrations from July to November and a decrease during winter months.

3.3 Spatio-temporal distribution pattern

We analyzed the model prediction for the temporal variation of *G. bulloides* in the North Atlantic. Figure 12 shows the model output of *G. bulloides* concentrations throughout the year in the North Atlantic. The maximum concentrations occur around 40° N during spring (March–April) and around 60° N during summer (June–July), following the typical phytoplankton bloom of North Atlantic (Colebrook, 1982; Litchman et al., 2006).

3.4 Sensitivity analysis: spatio-temporal distribution patterns with constant temperature

We run the foraminifera module with a constant temperature of 12°C to test the sensitivity of *G. bulloides* to other environmental parameters (mainly food availability). This temperature corresponds to the optimal temperature of this species assumed in the

model. Figure 13 shows the spatio-temporal distribution of *G. bulloides* in the North Atlantic for this experimental run. In general, absolute concentrations of *G. bulloides* are higher than in the standard run. The model shows again the highest concentrations first in the southern part (around 40°) and during summer the bloom is shifting to higher latitudes.

4 Discussion

4.1 Comparison with core-top data

In general, the global distribution patterns of foraminifera species predicted by the model are similar to those expected from core-top data.

The core-top data reflect the integrated flux through the water column, whilst our model reflects the situation in the mixed layer. Accordingly, we can expect some discrepancies between model and core-top distributions due to the different depth habitats of the species. But the five species of foraminifera simulated with our model live in most of the cases in the upper part of the water column, thus at a global scale we can expect a similar distribution. In addition, sedimentary assemblages may be altered by selective dissolution (Berger, 1968; Thunell and Honjo, 1981; Le and Thunell, 1996; Ditter and Henrich, 1999), by displacement through subsurface currents or by bioturbation processes (Bé, 1977; Bé and Hutson, 1977; Boltovskoy, 1994). Since we did not take into account any of the factors we also can expect some differences due to these processes.

N. pachyderma (sin.) is the only foraminifera species that growth in polar waters and also within sea-ice (Dieckmann et al., 1991; Spindler, 2006). The model output is in very good agreement with core-top data, showing very high concentrations at the poles and abscence or very low concentrations in the rest of the oceans. Darling et al. (2006) have shown that *N. pachyderma* (sin.) has many different cryptic species. As a consequence, the temperature tolerance of the southern populations is larger than that

of North Atlantic population. For the calibration we did not take into account the differenet genotypes, grouping all cryptic species as *N. pachyderma* (sin.). This will cause a discrepancy at the edge of the distribution in the North Atlantic, where the temperature tolerance range is narrower. The model output matches slighly better in the Southern Ocean, with a Root Mean Square Error of 9.3% in the northern hemisphere and 8.7% in the southern hemisphere. This confirms that our parametrization is based on temperature tolerance of the southern population. However, this difference is not large, and therefore we conclude that using this particular model and its parametrization, the different genotypes of *N. pachyderma* (sin.) can be grouped as a single species.

Model results for the distribution of *N. pachyderma* (dex.) were, in general, in agreement with data from sediment surface samples. The model simulates very high relative abundances (up to 90%) in the three eastern boundary upwelling systems. These high relative abundances in the equatorial Pacific and the Benguella upwelling are also reflected in the sediment samples. In comparison with core-top data, in the Atlantic Ocean results at mid latitudes were overestimated, while those at higher latitudes were underestimated. The pattern in the Pacific Ocean looks different. In the equatorial Pacific, north of the eastern boundary upwelling region, the model underestimates the relative abundance of *N. pachyderma* (dex.). At this region, the surface temperature is higher than the typical for *N. pachyderma* (dex.) (minimum temperatures above 22°C). It is possible that *N. pachyderma* (dex.) individuals present in these core-tops represent a population living below the mixed layer, as has been described in previous works (Murray, 1991; Pujol and Grazzini, 1995; Kuroyanagi and Kawahata, 2004), or that they are expatriated specimens from the upwelling region.

G. bulloides is common at mid-latitudes and subpolar waters, but it is also present in the subtropical waters of the Indian Ocean. It use to be related to high productivity areas (Hemleben et al., 1989; Sautter and Thunell, 1989; Guptha and Mohan, 1996). The model-generated global patterns for the Atlantic, Pacific and Southern Oceans agree with core-top data. The model, however, underestimates the abundance of *G. bulloides* in the North Indian Ocean. This underestimation could be due to the different *G. bu-*

lloides genotypes. The two warm water types are found mainly in tropical/subtropical regions, whereas cold water types are found in transitional to subpolar waters (Kucera and Darling, 2002). Žarić et al. (2005) studied the sensitivity of several planktonic foraminifera species to sea-surface temperature and concluded that the population of *G. bulloides* present in the tropical Indian Ocean comprises mainly the warm-water genotype. The parametrization of the model is done for a global scale without including the warm water type, and therefore the increased relative abundance of warm water *G. bulloides* in the tropical Indian Ocean is not captured by the model. The high concentrations simulated in the Arabian Sea are due to high phytoplankton concentration predicted by the ecosystem model. In the model, the temperature relation is approximated to a modified normal distribution. The modification of the normal distribution by the introduction of the food dependent relation (through the parameter *CT*) allows *G. bulloides* to grow in tropical waters. The model underestimated *G. bulloides* relative abundances in northwest of Africa as a result of its overestimation of *N. pachyderma* (dex.) relative abundance.

The model simulated global distribution pattern of *G. ruber* (white) shows a good agreement with the core-top data. The relative abundances in the Atlantic Ocean are comparable to core-top data, while in the Indian Ocean abundances are overestimated. There are few core-top data from the North Pacific and although their low number question the accuracy of the model validation, they do appear to support the model.

Both core-top and model output show that the distribution of *G. sacculifer* is limited to tropical waters. The model captures well the distribution patterns in the Atlantic Ocean and the East Pacific. The predicted relative abundances of *G. sacculifer* in the Indian and West Pacific Oceans are underestimated in the model; the distribution seen in the sediment data shows a wider spatial coverage than in the simulated results. This could be due to the competition exerted by *G. ruber*. *G. ruber* is overestimated in the Indian Ocean and therefore the competition exerting upon the other species is overstated.

4.2 Comparison with sediment-trap data

In general, the seasonal signal of species concentrations are similar to sediment-trap records of most of the species.

Figure 7 shows some examples of *N. pachyderma* (sin.) in the northern North Atlantic, Northwest Pacific and Wedell Sea. In the sediment-trap data from the northern North Atlantic (Fig. 7a) during the last two years of the sampling period the timing of the seasonal peak coincides with the model prediction, whereas in the first sampled year is out of phase. In the Northwest Pacific (station PAPA, Fig. 7b), there is a good agreement between data and model output, showing maximum seasonal values between March and July. During the winter of 1985 there is second bloom not predicted by the model. We do not know if this phenomenon is a reoccurring feature since there are data gaps for this period in other years. In the last location, the Wedell Sea (Fig. 7c), the data do not show evidence of any bloom, probably due to the variability of ice dynamic in the area. Despite the interannanual variabilities, the intraannual variability matches well with the observed data.

The seasonal pattern of predicted concentration for *N. pachyderma* (dex.) matches fairly well with the trap record in most of the locations. In the Northwest Pacific (Fig. 8b) sediment-trap data was only available for one year. These data gaps make the model validation complicated, since we can not confirm patterns as typical for this region. Nevertheless, the model predicts a similar seasonal variation to that seen in the limited sediment-trap data available. The observational data of Walvis Ridge (Fig. 8c) does no show a clear seasonal pattern during the first year of the sampling (1989). However, during the last two years there is an increase of the population during autumn (from September to December). This location is very close to Benguella upwelling system, and therefore is strongly influenced by the variability of the upwelling intensity and wind system. The model output reflects a smoother situation, but the timing of the bloom matches well with those reflected by the trap data. In the Subantartic Zone (46.76° S 142.07° E, Fig. 8d), the model predicts effectively the increase of *N. pachyderma* (dex.)

population seen in the trap-data during the first austral summer. There is no evidence of increase of *N. pachyderma* (dex.) flux during the second summer, but the trap data are no longe enough to confirm the absence of the summer peak.

The model prediction capability of *G. bulloides* varies between locations. At some locations, for example in the Japan Trench (34.16° N 141.98° E), the predictions correspond to the observational data, with a single annual peak during spring. At the station located at the Walvis ridge (20.05° S 9.16° E), close to the coastal upwelling zone, the model predicts successfully the bimodal pattern, with the main bloom in the austral spring (October–November) and a secondary bloom in fall (May–June). Contrarily, in some other locations the result differed significantly from sediment-trap data (Fig. 9). For example, the in Peru Chile current the model predicts two annual peaks, while the sediment-trap data clearly show a single peak during the austral summer (from December to end of January). This station is situated on the eastern boundary upwelling system of south America and therefore the environmental conditions and ecological successions are more complicated than in open ocean. In this region the model is not able to predict the pattern shown by the sediment-trap data. It should be noted that the sediment-trap data exist only for a single year. It is, therefore, possible that this data does not reflect the true typical annual pattern. In the subarctic station of the Northwest Pacific (39.01° N 147.00° E), along the boundary of the Kuroshio and Oyashio currents, sediment-trap data showed the variability in a sampling period of two years. During the second sampling year (1999) the data and the model output fit well with two maxima, one during the winter months (December–January) and a second one in early summer. During the first year (1998) the summer peak was absent. This station is located in the subarctic front, with a complex hydrography and mixing of several water masses (Mohiuddin et al., 2002). The absence of the summer peak could be related to interannual changes in water sources and water column conditions due to interaction between subarctic water masses (Oyashio Current) and subtropical water masses at this site.

In general, the sediment-trap data of *G. ruber* (white) show less variability than *N. pachyderma* and *G. bulloides* (Fig. 10). The seasonal pattern of *G. ruber* (white) at Cape

Blanc (21.15° N 20.69° W), located to the upwelling zone of the cold Canary Current, shows dominant flux-maxima in fall (September–December), with variable amplitudes (Fig. 10a). The model predicts a wider peak, from summer to winter, matching well with the timing of sediment-trap data (except for the last year, when the fall bloom is missing). In the western equatorial Atlantic (7.51° S 28.03° W), and Northwest Pacific (25.00° N 136.99° E) sediment-trap data show quite an irregular pattern. Despite this, it is possible to distinguish a bimodal pattern, with one peak in June–July and a second in November–December. During the second year the winter peak in the western equatorial Atlantic is absent. At these stations the model does not predict the expected seasonal cycle. Because the sediment-trap data do not show a clear annual cycle, we can not confirm this pattern as the typical annual pattern, and therefore the validation at this site is not highly reliable. The site at the Bay of Bengal, in the northern Indian Ocean, shows less variability both in sediment-trap data and in the model output. The Bay of Bengal is affected by a monsoonal climatic regime, with the southwest monsoon (June to August) creating a small upwelling cell along the eastern coast of India; and the northeast monsoon (November to April) forming a moderately developed Cyclonic Gyre (Guptha et al., 1997). Sediment-trap data does not show prominent maxima associated with monsoonal seasons, but even if the variability is quite low, it shows three flux maxima: during December to January, May to June and August to September. Nevertheless, these oscillations are very small compared to the other sites, and the low variability is reflected in the model output.

Most of the sites from which sediment-trap data are available for, the model underpredicts the concentrations of *G. sacculifer*. In tropical waters, most of the sediment-trap data are located in high productivity areas or close to upwelling zones. *G. sacculifer* is parametrized to be more abundant in low productivity regions, and therefore in most of the sites the concentrations predicted by the model are too low. When the concentration is close to the threshold value the mixed-layer depth plays a bigger role than the population dynamic itself and therefore we can not do a correct comparison. We show some examples where the model predicts sufficient concentrations

for a proper comparison (Fig. 11). For example, in the Bay of Bengal, the model is in good agreement with the sediment-trap data. In the northern Bay of Bengal both sedimnent-trap data and model result show little variability throughout the year indicating that the monsoonal system does not substantially affect the *G. sacculifer* population. In the central Bay of Bengal the population increases during summer months, probably due to the southwest monsoon (June to August), which dominates the northern Indian Ocean (Cullen, 1981). During the southwest monsoon surface circulation is dominated by a wind-driven anticyclonic gyre, generating a strong boundary current and a small upwelling cell along the eastern coast of India. Unlike in the northern Bay of Bengal, the foraminiferal population in the central Bay of Bengal is affected by hydrographic changes associated to the monsoon seasons Guptha et al. (1997). The Brasil Basin (western equatorial Atlantic, Fig. 11c) is characterized by representing typical oligotrophic open-ocean conditions (Fischer and Wefer, 1996). This is reflected in sediment-trap data, which indicates very low fluxes of *G. sacculifer*. The model output also shows very low concentrations, but the small variations seem to be out of phase with respect to the trap data, possibly because the values are close to the threshold value and at this point the physical processes start to dominate over the ecology. In the Arabian Sea, planktonic foraminifera reach highest production rates at monsoon seasons responding to hydrographical changes related to the monsoons: southwest monsoon (June–August), resulting in a upwelling cell in the coastline of Somalia and Oman; and northeast monsoon (November–April) which suppresses the upwelling (Curry et al., 1992). During both monsoonal periods, the depth of the mixed layer increases and nutrient-rich water is injected into the euphotic zone (Monterey and Levitus, 1997). *G. sacculifer* has been identified as typical for northeast monsoon rather than the southwest monsoon seasons (Curry et al., 1992; Ishikawa and Oda, 2007), although the sediment-trap data we used show a bimodal pattern related to both monsoon seasons, with a prominent increase during the southwest monsoon of 1987. The model cannot predict a clear response to the monsoonal system. This could be due to the fact that the ecosystem model is unable to predict a bimodal pattern, related to both monsoon

seasons, in the zooplankton distribution of this region, and *G. sacculifer* depends on zooplankton availability.

4.3 Model experiment with constant mixed-layer temperature

When running the foraminifera module with a constant temperature of 12°C the result for *G. bulloides* in the North Atlantic still showed highest concentrations at low latitudes during spring and maximum concentrations at higher latitudes in June, linked to the phytoplankton bloom succession in the the North Atlantic. This indicates that the temperature is not the only controlling factor, but the food supply plays an important role in the distribution pattern of this species. The experiment confirms the results of Ganssen and Kroon (2000), who from isotopic studies on North Atlantic surface sediments concluded that *G. bulloides* reflects temperatures of a northward migrating spring bloom. The model can reflect its preference for high productivity environments, as has been suggested by different authors (e.g., Bé and Tolderlund, 1971; Bé, 1977; Duplessy et al., 1981; Prell and Curry, 1981; Guptha and Mohan, 1996).

5 Summary and conclusions

A foraminifera model at a global scale has been developed and its results compared with core-top and sediment-trap data. The model presented here globally predicts monthly planktonic foraminifera concentrations for 5 species: *N. pachyderma* (sin.), *N. pachyderma* (dex.), *G. bulloides*, *G. ruber* (white) and *G. sacculifer*. It is a non-linear dynamic model simulating growth rate of the foraminifera populations coupled to a ecosystem model (Moore et al., 2002a), which calculates food availability for foraminifera.

Overall, the global distribution patterns of the predicted species are similar to core-top data. In the case of *G. bulloides*, several genotypes included in this group appear to be adapted to different environmental conditions, complicating the modeling at a global

scale. Incorporation of more species, hence, a better representation of competition, could further improve the quality of the model.

Modeled seasonal variation agrees well with sediment-trap records in most of the locations for *N. pachyderma* (sin), *N. pachyderma* (dex.) and *G. bulloides*. *G. ruber* and *G. sacculifer* show, in general, lower concentrations and little variability at all sites. The lower variability is reflected in the model, but it fails to adequately describe the the small scale variations in several locations. Due to the forcing, interannual variations can not be elucidated by our model.

The experimental run with constant temperature of 12°C shows that temperature is not the only controlling factor in the distribution pattern of some species of planktonic foraminifera, but food availability (primary production in case of *G. bulloides*) is also an important factor controlling the habitat of some species.

Our model provides a tool to predict seasonal variations of five foraminifera species at different environments. With this approach the model has the potential to identify seasonal flux signals and to quantify the seasonal bias in foraminifera-based proxy records.

Acknowledgements. We appreciate the contribution and helpful comments of R. Schiebel, M. Peck and A. Bisset. Thanks also to M. Prange and T. Laepple for the analytical assistance. A special thanks to A. Manschke for the computer support. This project has been carried out with the financial support of DFG (Deutsche Forschungsgemeinschaft) as part of the European Graduate Collegue "Proxies in Earth History" (EUROPROX).

References

Anderson, O. R., Spindler, M., Be, A. W. H., and Hemleben, C.: Trophic activity of planktonic foraminifera, J. Mar. Biol. Assoc. U.K., 59, 791–799, 1979. 4328

Arnold, A. J. and Parker, W. C.: Biogeography of planktonic Foraminifera, in: Modern Foraminifera, edited by: Gupta, B. S. K., Dortrecht, Boston, London, 103–122, 1999. 4328, 4330

Asahi, H. and Takahashi, K.: A 9-year time-series of planktonic foraminifer fluxes and environmental change in the Bering sea and the central subarctic Pacific Ocean, 1990–1999, Prog. Oceanogr., 72, 343–363, 2007. 4335, 4362

Bé, A. W. H. and Hamilton, W. H.: Ecology of Recent planktonic foraminifera, Micropal., 13, 87–106, 1967. 4325

Bé, A. W. H. and Tolderlund, D. S.: Distribution and ecology of living planktonic foraminifera in surface waters of the Atlantic and Indian Oceans, in The Micropalaeontology of Oceans, edited by: Funnell, B. M. and Riedel, W. R., 105–149, Cambridge University Press, 1967. 4325, 4349

Bé, A. W. H.: An ecological, zoogeographic and taxonomic review of recent planktonic foraminifera, in: Oceanic Micropalaeontology, edited by: Ramsay, A. T. S., 1–100, Academic Press Inc., London, 1977. 4334, 4336, 4342, 4349

Bé, A. W. H. and Hutson, W. H.: Ecology of planktonic foraminifera and biogeographic patterns of life and fossil assemblages in the Indian Ocean, Micropal., 23, 369–414, 1977. 4342

Bé, A. W. H., Caron, D. A., and Anderson, O. R.: Effects of feeding frequency on life processes of the planktonic foraminifer *Globigerinoides sacculifer* in laboratory culture, J. Mar. Biol. Assoc. U.K., 61, 257–277, 1981. 4329

Bé, A. W. H., Bishop, J. K. B., Sverdlove, M. S., and Gardner, W. D.: Standing stock, vertical distribution and flux of planktonic Foraminifera in the Panama Basin, Mar. Micropal., 9, 307–333, 1985. 4336

Berger, W. H.: Planktonic foraminifera: selective solution and paleoclimatic interpretation, Deep-Sea Res., 15, 31–43, 1968. 4342

Bijma, J., Faber, W. W. J., and Hemleben, C.: Temperature and salinity limits for growth and survival of some planktonic foraminifers in laboratory cultures, J. Foramin. Res., 20, 95–116, 1990. 4325, 4330

Bishop, J. K. B. and Rossow, W. B.: Spatial and temporal variability of global surface solar irradiance, J. Geophys. Res., 96, 16 839–16 858, 1991. 4333

Boltovskoy, D.: The sedimentary record of pelagic biogeography, Prog. Oceanogr., 34, 135–160, 1994. 4342

Bradshaw, J. S.: Ecology of living planktonic foraminifera in the North and equatorial Pacific Ocean, Cushman Foundation for Foraminiferal Research Contribution, 10, 25–64, 1959. 4336

Caron, D. A. and Bé, A. W. H.: Predicted and observed feeding rates of the spinose planktonic

foraminifer Globigerinoides sacculifer, B. Mar. Sci., 35, 1–10, 1984. 4328
Cavalieri, D., Gloerson, P., and Zwally, J.: DMSP SSM/I daily polar gridded sea ice concentrations, October 1998 to September 1999, edited by: Maslanik, J. and Stroeve, J., National Snow and Ice Data Center, Boulder, CO, Digital media, 1990. 4333
CLIMAP Project Members: The surface of the ice-age earth, Science, 191, 1131–1137, 1976. 4325
Colebrook, J. M.: Continuous Plankton Records: seasonal variations in the distribution and abundance of plankton in the North Atlantic and the North Sea, J. Plankton Res., 4, 435–462, 1982. 4341
Cullen, J. L.: Microfossil evidence for changing salinity patterns in the Bay of Bengal over the last 20,000 years, Palaeogeogr. Palaeocl., 35, 315–356, 1981. 4348
Curry, W. B., Ostermann, D. R., Guptha, M. V. S., and Ittekkot, V.: Foraminiferal production and monsoonal upwelling in the Arabian Sea: evidence from sediment traps, in: Upwelling Systems: Evolution Since the Early Miocene, edited by: Summerhayes, C. P., Prell, W. L., and Emeis, K. C., 93–106, The Geological Society, London, 1992. 4348, 4362, 4382
Darling, K. F., Wade, C. M., Kroon, D., Leigh Brown, A. J., and Bijma, J.: The diversity and distribution of modern planktonic foraminiferal small subunit ribosomal RNA genotypes and their potential as tracers of present and past ocean circulations, Paleoceanography, 14, 3–12, 1999. 4331, 4336
Darling, K. F., Wade, C. M., Stewart, I. A., Kroon, D., Dingle, R., and Leigh Brown, A. J.: Molecular evidence for genetic mixing of Arctic and Antarctic subpolar populations of planktonic foraminifers, Nature, 405, 43–47, 2000. 4331, 4336
Darling, K. F., Kucera, M., Wade, C. M., von Langen, P., and Pak, D.: Seasonal distribution of genetic types of planktonic foraminifer morphospecies in the Santa Barbara Channel and its paleoceanographic implications, Paleoceanography, 18, 1032, doi:10.1029/2001PA000723, 2003. 4331, 4336
Darling, K. F., Kucera, M., Kroon, D., and Wade, C. M.: A resolution for the coiling direction paradox in *Neogloboquadrina pachyderma*, Paleoceanography, 21, 2011, doi:10.1029/2005PA001189, 2006. 4342
Deuser, W. G. and Ross, E. H.: Seasonally abundant planktonic foraminifera of the Sargasso Sea: succession, deep-water fluxes, isotopic compositions, and paleoceanographic implications, J. Foramin. Res., 19, 268–293, 1989. 4325
Dieckmann, G. S., Spindler, M., Lange, M. A., Ackley, S. F., and Eicken, H.: Antarctic sea ice:

a habitat for the foraminifer *Neogloboquadrina pachyderma*, J. Foramin. Res., 21, 182–189, 1991. 4331, 4336

Dittert, N. and Henrich, R.: Carbonate dissolution in the South Atlantic Ocean: evidence from ultrastructure breakdown in Globigerina bulloides, Deep-Sea Res. I, 47, 603–620, 1999. 4342

Donner, B. and Wefer, G.: Flux and stable isotope composition of *Neogloboquadrina pachyderma* and other planktonic foraminifers in the Southern Ocean (Atlantic sector), Deep-Sea Res. I, 41, 1733–1743, 1994. 4362, 4370

Duplessy, J. C., Delibrias, G., Turon, J. L., Pujol, C., and Duprat, J.: Deglacial warming of the Northeastern Atlantic Ocean: correlation with the paleoclimatic evolution of the European continent, Palaeogeogr. Palaeocl., 35, 121–144, 1981. 4334, 4336, 4349

Edwards, A. M. and Yool, A.: The role of higher predation in plankton population models, J. Plankton Res., 22, 1085–1112, 2000. 4332

Eguchi, N. O., Kawahata, H., and Taira, A.: Seasonal Response of Planktonic Foraminifera to Surface Ocean Condition: Sediment Trap Results from the Central North Pacific Ocean, J. Oceanogr., 55, 681–691, 1999. 4325

Fischer, G. and Wefer, G.: Long-term Observation of Particle Fluxes in the Eastern Atlantic: Seasonality, Changes of Flux with Depth and Comparison with the Sediment Record, in: The South Atlantic: Present and Past Circulation, edited by: Wefer, G., Berger, W. H., Siedler, G., and Webb, D. J., 325–344, Springer-Verlag, Berlin Heidelberg, 1996. 4348, 4362, 4373, 4376, 4379, 4382

Fischer, G., Donner, B., Ratmeyer, V., Davenport, R., and Wefer, G.: Distinct year-to-year particle flux variations off Cape Blanc during 1988–1991: Relation to δ^{18}O-deduced sea-surface temperatures and trade winds, J. Mar. Res., 54, 73–98, 1996. 4362, 4379, 4382

Ganssen, G. M. and Kroon, D.: The isotopic signature of planktonic foraminifera from NE Atlantic surface sediments: implications for the reconstruction of past oceanic conditions, J. Geol. Soc., 157, 693–699, 2000. 4326, 4349

Gent, P. R., Bryan, F. O., Danabasoglu, G., Doney, S. C., Holland, W. R., Large, W. G., and McWilliams, J. C.: The NCAR climate system model global ocean component, J. Climate, 11, 1287–1306, 1998. 4333

Giraudeau, J.: Planktonic foraminiferal assemblages in surface sediments from the southwest African continental margin, Mar. Geol., 110, 47–62, 1993. 4336

Guptha, M. V. S. and Mohan, R.: Seasonal variability of the vertical fluxes of *Globigerina bulloi-*

des (d Orbigny) in the northern Indian Ocean, Mitt. Geol.-Paläont. Inst. Univ. Hamburg, 79, 1–17, 1996. 4343, 4349, 4362, 4379, 4382

Guptha, M. V. S., Curry, W. B., Ittekkot, V., and Muralinath, A. S.: Seasonal variation in the flux of planktic foraminifera: Sediment trap results from the Bay of Bengal, northern Indian Ocean, J. Foramin. Res., 27, 5–19, 1997. 4347, 4348, 4362, 4379, 4382

Haake, B., Ittekkot, V., Rixen, T., Ramaswamy, V., Nair, R. R., and Curry, W. B.: Seasonality and interannual variability of particle fluxes to the deep Arabian Sea, Deep-Sea Res. I, 40, 1323–1344, 1993. 4362, 4382

Hebbeln, D., Marchant, M., and Wefer, G.: Seasonal variations of the particle flux in the Peru-Chile current at 30° S under normal and El Niño conditions, Deep-Sea Res. II, 47, 2101–2128, 2000. 4362, 4376

Hemleben, C., Spindler, M., Breitinger, J., and Deuser, W. G.: Field and laboratory studies of the ontogeny and ecology of *Globorotalia truncatulinoides* and *G. hirsuta* in the Sargasso Sea, J. Foramin. Res., 15, 254–272, 1985. 4328

Hemleben, C., Spindler, M., and Anderson, O. R.: Modern Planktonic Foraminifera, Springer-Verlag, New York, 1989. 4328, 4329, 4336, 4337, 4343

Ishikawa, S. and Oda, M.: Reconstruction of Indian monsoon variability over the past 230,000 years: Planktic foraminiferal evidence from the NW Arabian Sea open-ocean upwelling area, Mar. Micropal., 63, 143–154, 2007. 4348

Jensen, S.: Planktische Foraminiferen im Europaischen Nordmeer: Verbreitung und Vertikalfluss sowie ihre Entwicklung während der letzten 15000 Jahre, Berichte SFB 313, Univ. Kiel, 75, 105 pp., 1998. 4362, 4370, 4373

Kiefer, T.: Productivitätund Temperaturen im subtropischen Nordatlantic: zyklische und abrupte Veränderungen im späten Quartär, Berichte – Reports, Geol.-Paläont. Inst., Univ. Kiel, 90, 1–127, 1998. 4325

King, A. L. and Howard, W. R.: Seasonality of foraminiferal flux in sediment traps at Chatham Rise, SW Pacific: implications for paleotemperature estimates, Deep-Sea Res. I, 48, 1687–1708, 2001. 4326

King, A. L. and Howard, W. R.: Planktonic foraminiferal flux seasonality in Subantarctic sediment traps: A test for paleoclimate reconstructions, Paleoceanography, 18, 1019, doi:1010.1029/2002PA000839, 2003a. 4325, 4362, 4373

King, A. L. and Howard, W. R.: Seasonal Subantarctic Planktonic Foraminiferal Flux Data, available from the IGBP PAGES/World Data Center for Paleoclimatology (http://www.ngdc.noaa.

gov/paleo), Data Contribution Series # 2003-022., NOAA/NGDC Paleoclimatology Program, Boulder CO, 2003b. 4362, 4373
Kucera, M. and Darling, K. F.: Cryptic species of planktonic foraminifera: their effect on paleoceanographic reconstructions, Philos. Tr. Roy. Soc. A, 360, 695–718, 2002. 4331, 4336, 4344
Kuroyanagi, A., Kawahata, H., Nishi, H., and Honda, M. C.: Seasonal changes in planktonic foraminifera in the northwestern North Pacific Ocean: sediment trap experiments from subarctic and subtropical gyres, Deep-Sea Res. II, 49, 5627–5645, 2002. 4362, 4373
Kuroyanagi, A. and Kawahata, H.: Vertical distribution of living planktonic foraminifera in the seas around Japan, Mar. Micropal., 53, 173–196, 2004. 4343
Le, J. and Thunell, R. C.: Modelling planktic foraminiferal assemblage changes and application to sea surface temperature estimation in the western equatorial Pacific Ocean, Mar. Micropal., 28, 211–229, 1996. 4342
Lea, D. W.: Trace elements in foraminiferal calcite, in: Modern foraminifera, edited by: Gupta, B. S. K., Dortrecht, Boston, London, 259–277, 1999. 4325
Levitus, S.: Climatological Atlas of the World Ocean, NOAA Professional Paper No. 13, 191 pp., U.S. Government Printing Office, Washington, D.C., World Ocean Atlas 1998 data provided by the NOAA-CIRES Climate Diagnostics Center, Boulder, CO, USA, from their Web site at http://www.cdc.noaa.gov/, 1982. 4333
Litchman, E., Klausmeier, C. A., Miller, J. R., Schofield, O. M., and Falkowski, P. G.: Multi-nutrient, multi-group model of present and future oceanic phytoplankton communities, Biogeosciences, 3, 585–606, 2006, http://www.biogeosciences.net/3/585/2006/. 4341
Malmgren, B. A., Kucera, M., Nyberg, J., and Waelbroeck, C.: Comparison of statistical and artificial neural network techniques for estimating past sea surface temperature from planktonic foraminifer census data, Paleoceanography, 16, 520–530, 2001. 4325
Marchant, M., Hebbeln, D., and Wefer, G.: Seasonal flux patterns of planktic foraminifera in the Peru-Chile Current, Deep-Sea Res. I, 45, 1161–1185, 1998. 4362, 4365, 4366, 4367, 4376
Marchant, M., Hebbeln, D., Giglio, S., Coloma C., and Gonzalez, H.: Seasonal and interannual variability in the flux of planktic foraminifers in the southern Humboldt Current System off central Chile, Deep-Sea Res. II, 51, 2441–2455, 2004. 4335
Martinez, J. I., Taylor, L., Deckker, P., and Barrows, T.: Planktonic foraminifera from the eastern Indian Ocean: distribution and ecology in relation to the Western Pacific Warm Pool (WPWP),

Mar. Micropal., 34, 121–151, 1998. 4334, 4364, 4368
Michaels, A. F., Caron, D. A., Swanberg, N. R., and Howse, F. A.: Planktonic sarcodines (Acantharia, Radiolaria, Foraminifera) in surface waters near Bermuda: abundance, biomass and vertical flux, J. Plankton Res., 17, 131–163, 1995. 4334
Mohiuddin, M. M., Nishimura, A., Tanaka, Y., and Shimamoto, A.: Regional and interannual productivity of biogenic components and planktonic foraminiferal fluxes in the northwestern Pacific Basin, Mar. Micropal., 45, 57–82, 2002. 4346, 4362, 4376, 4379
Mohiuddin, M. M., Nishimura, A., Tanaka, Y., and Shimamoto, A.: Seasonality of biogenic particle and planktonic foraminifera fluxes: response to hydrographic variability in the Kuroshio Extension, northwestern Pacific Ocean, Deep-Sea Res. I, 51, 1659–1683, 2004. 4335
Monterey, G. and Levitus, S.: Seasonal variability ofmixed layer depth for the world ocean, NOAA Atlas NESDIS 14, US Government Printing Office, Washington, D.C., 1997. 4333, 4348
Moore, J. K., Doney, S. C., Kleypas, J. A., Glover, D. M., and Fung, I. Y.: An intermediate complexity marine ecosystem model for the global domain, Deep-Sea Res. II, 49, 403–462, 2002a. 4327, 4332, 4333, 4349
Moore, J. K., Doney, S. C., Glover, D. M., and Fung, I. Y.: Iron cycling and nutrient-limitation patterns in surface waters ofthe World Ocean, Deep-Sea Res. II, 49, 463–507, 2002b. 4327, 4333
Morey, A. E., Mix, A. C., and Pisias, N. G.: Planktonic foraminiferal assemblages preserved in surface sediments correspond to multiple environment variables, Quat. Sci. Rev., 24, 925–950, 2005. 4325
Motoyoshi, O. and Makoto, Y.: Sediment trap results from the Japan trench in the Kuroshio domain: seasonal variations in the planktic foraminiferal flux, J. Foramin. Res., 35, 315–326, 2005. 4335
Mulitza, S., Dürkoop, A., Hale, W., Wefer, G., and Niebler, H. S.: Planktonic foraminiferaa as recorders of past surface-water stratification, Geology, 25, 335–338, 1997. 4325
Mulitza, S., Wolff, T., Pätzold, J., Hale, W., and Wefer, G.: Temperature sensitivity of planktic foraminifera and its influence on the oxygen isotope record, Mar. Micropal., 33, 223–240, 1998. 4325
Murray, J. W.: Ecology, and distribution of planktonic foraminifera, in: Biology of foraminfera, edited by: Lee, J. J. and Anderson, O. R., Academic Press, Harcourt, 255–284, 1991. 4329, 4334, 4343

Niebler, H. S., Arz, H. W., Donner, B., Mulitza, S., Patzold, J., and Wefer, G.: Sea surface temperatures in the equatorial and South Atlantic Ocean during the last glacial maximum (23–19 ka), Paleoceanography, 18, 1069, doi:1010.1029/2003PA000902, 2003. 4326

Nodder, S. D. and Northcote, L. C.: Episodic particulate fluxes at southern temperate mid-latitudes (42–45° S) in the Subtropical Front region, east of New Zealand, Deep-Sea Res. I, 48, 833–864, 2001. 4362

Oda, M. and Yamasaki, M.: Sediment trap results from the Japan Trench in the Kuroshio domain: seasonal variations in the planktic foraminiferal flux, J. Foramin. Res., 35, 315–326, 2005. 4362, 4376

Ortiz, J. D., Mix, A. C., and Collier, R. W.: Environmental control of living symbiotic and asymbiotic foraminifera of the California Current, Paleoceanography, 10, 987–1009, 1995. 4325

Pearson, P. N. and Palmer, M. R.: Atmospheric carbon dioxide concentrations over the past 60 million years, Nature, 406, 695–699, 2000. 4325

Peeters, F., Ivanova, E., Conan, S., Brummer, G. J., Ganssen, G., Troelstra, S., and van Hinte, J.: A size analysis of planktic foraminifera from the Arabian Sea, Mar. Micropal., 36, 31–63, 1999. 4334

Peinert, R., Antia, A. N., Bauerfeind, E., Haupt, O., Krumbholz, M., Peeken, I., Bodungen, B. V., Ramseier, R., Voss, M., and Zeitzschel, B.: Particle Flux Variability in the Polar and Atlantic Biogeochemical Provinces of the Nordic Seas, in: The Northern North Atlantic: A Changing Environment, edited by: Schäfer, P., Ritzrau, W., Schlüter, M., and Thiede, J., 53–68, Springer, Berlin, 2001. 4362

Pflaumann, U., Duprat, J., Pujol, C., and Labeyrie, L. D.: SIMMAX: A modern analog technique to deduce Atlantic sea surface temperatures from planktonic foraminifera is deep-sea sediments, Paleoceanography, 11, 15–35, 1996. 4325, 4334, 4364, 4365, 4366, 4367, 4368

Pflaumann, U., Sarnthein, M., Chapman, M., d'Abreu, L., Funnell, B., Huels, M., Kiefer, T., Maslin, M., Schulz, H., Swallow, J., van Kreveld, S., Vautravers, M., Vogelsang, E., and Weinelt, M.: Glacial North Atlantic: Sea-surface conditions reconstructed by GLAMAP 2000, Paleoceanography, 18, 1065, doi:1010.1029/2002PA000774, 2003. 4326

Prell, W. L. and Curry, W. B.: Faunal and isotopic indices of monsoonal upwelling: Western Arabian Sea, Oceanologica Acta, 4, 91–95, 1981. 4336, 4349

Prell, W. L., Martin, A., Cullen, J., and Trend, M.: The Brown University Foraminiferal Data Base, IGBP PAGES/World Data Center-A for Paleoclimatology, Data Contribution Series # 1999-027, NOAA/NGDC Paleoclimatology Program, Boulder CO, USA, 1999. 4334, 4364,

4365, 4366, 4367, 4368
Pujol, C. and Grazzini, C. V.: Distribution patterns of live planktic foraminifers as related to regional hydrography and productive systems of the Mediterranean Sea, Mar. Micropal., 25, 187–217, 1995. 4343
Reynolds, L. and Thunell, R. C.: Seasonal succession of planktonic foraminifera in the subpolar North Pacific, J. Foramin. Res., 15, 282–301, 1985. 4362, 4370
Rohling, E. J. and Cooke, S.: Stable oxygen and carbon isotopes in foraminiferal carbonate shells in: Modern foraminifera, edited by: Gupta, B. S. K., Dortrecht, Boston, London, 239–258, 1999. 4325
Rossow, W. B. and Schiffer, R. A.: ISCCP cloud data products, B. Am. Meteorol. Soc., 72, 2–20, 1991. 4333
Sautter, L. R. and Thunell, R. C.: Seasonal succession of planktonic foraminifera: results from a four-year time-series sediment trap experiment in the northeast Pacific, J. Foramin. Res., 19, 253–267, 1989. 4343, 4362, 4370
Schiebel, R., Hiller, B., and Hemleben, C.: Impacts of storms on recent planktic foraminiferal test production and $CaCO_3$ flux in the North Atlantic at 47.8° N, 20.8° W (JGOFS), Mar. Micropal., 26, 115–129, 1995. 4328
Schiebel, R., Waniek, J., Bork, M., and Hemleben, C.: Planktic foraminiferal production stimulated by chlorophyll redistribution and entrainment of nutrients, Deep-sea Res. I, 48, 721–740, 2001. 4325, 4336
Schmidt D. N.: Size variability in planktic foraminifera, PhD thesis, ETH No. 14578, 2002.
Schnack-Schiel, S. B., Dieckmann, G. S., Gradinger, R., Melnikov, I. A., Spindler, M., and Thomas, D. N.: Meiofauna in sea ice of the Weddell Sea (Antarctica), Polar Biol., 24, 724–728, 2001. 4325, 4336
Schulz, H., Von Rad, U., and Ittekkot, V.: Planktic foraminifera, particle flux and oceanic productivity off Pakistan, NE Arabian Sea: modern analogues and application to the paleoclimatic record, in: The Tectonic and Climatic Evolution of the Arabian Sea Region, edited by: Clift, P. D., Kroon, D., Gaedicke, C., and Craig, J., Geol. Soc. Spec. Publ., 195, 499–516, 2002. 4335, 4362
Simstich, J.: Die ozeanische Decksechicht des Europäischen Nordmeers im Abbild stabiler Isotope vo Kalkgehüsen unterschiedlicher Planktonforaminiferenarten, Berichte-Reports, Inst. fr Geowiss., Univ. Kiel, 2, 1–96, 1999. 4326
Spindler, M., Hemleben, C., Salomons, J. B., and Smit, L. P.: Feeding behavior of some plank-

tonic foraminifers in laboratory cultures, J. Foramin. Res., 14, 237–249, 1984. 4328
Spindler, M. and Dieckmann, G. S.: Distribution and Abundance of the Planktic Foraminifer *Neogloboquadrina pachyderma* in Sea Ice of the Weddell Sea (Antarctica), Polar Biol., 5, 185–191, 1986.
Spindler, M.: On the salinity tolerance of the planktonic foraminifer *Neogloboquadrina pachyderma* from Antarctic sea ice, Proc. NIPR Symp. Polar Biol., 9, 85–91, 1996. 4331, 4336
Steele, J. H. and Henderson, E. W.: The role of predation in plankton models, J. Plankton Res., 14, 157–172, 1992. 4332
Stewart, I. A., Darling, K. F., Kroon, D., Wade, C. M., and Troelstra, S. R.: Genotypic variability in subarctic Atlantic planktic foraminifera, Mar. Micropal., 43, 143–153, 2001. 4331, 4336
Takahashi, K. and Be, A. W. H.: Planktonic foraminifera: factors controlling sinking speed, Deep-Sea Res., 31, 1477–1500, 1984. 4335
Tedesco, K. A. and Thunell, R. C.: Seasonal and interannual variations in planktonic foraminiferal flux and assemblage composition in the Cariaco Basin, Venezuela, J. Foramin. Res., 33, 192–210, 2003. 4335, 4362
Tegen, I. and Fung, I. Y.: Modeling of mineral dust in the atmosphere: sources, transport, and optical thickness, J. Geophys. Res., 99, 22 897–22 914, 1994. 4333
Tegen, I. and Fung, I. Y.: Contribution to the atmospheric mineral aerosol load from land surface modification, J. Geophys. Res., 100, 18 707–18 726, 1995. 4333
Thunell, R. C. and Honjo, S.: Calcite dissolution and the modification of planktonic foraminiferal assemblages, Mar. Micropal., 6, 169–182, 1981. 4342
Thunell, R. C. and Reynolds, L. A.: Sedimentation of planktonic foraminifera: seasonal changes in species flux in the Panama Basin, Micropaleontology, 30, 243–262, 1984. 4336
Tian, J., Wang, P., Chen, R., and Cheng, X.: Quaternary upper ocean thermal gradient variations in the South China Sea: Implications for east Asian monsoon climate, Paleoceanography, 20, 4007, doi:10.1029/2004PA001115, 2005. 4335, 4362
Tolderlund, D. S. and Be, A. W. H.: Seasonal distribution of planktonic Foraminfera in the western North Atlantic, Micropalaeontology, 17, 297–329, 1971. 4336
Trull, T. W., Bray, S. G., Manganini, S. J., Honjo, S., and Francois, R.: Moored sediment trap measurements of carbon export in the Subantarctic and Polar Frontal Zones of the Southern Ocean, south of Australia, J. Geophys. Res., 106, 31 489–31 510, 2001. 4362, 4373
Waelbroeck, C., Mulitza, S., Spero, H., Dokken, T., Kiefer, T., and Cortijo, E.: A global compilation of late Holocene planktonic foraminiferal δ^{18}O: relationship between surface water

temperature and δ^{18}O, Quat. Sci. Rev., 24, 853–868, 2005. 4326

Watkins, J. M., Mix, A. C., and Wilson, J.: Living planktic foraminifera: tracers of circulation and productivity regimes in the central equatorial Pacific, Deep-Sea Res. II, 43, 1257–1282, 1996. 4325, 4329, 4337

Watkins, J. M. and Mix, A. C.: Testing the effects of tropical temperature, productivity, and mixed-layer depth on foraminiferal transfer functions, Paleoceanography, 13, 96–105, 1998. 4325, 4334, 4337

Wefer, G.: Particle Flux in the Ocean: Effects of Episodic Production, in: Productivity of the Ocean: Present and Past, edited by: Berger, W. H., Smetacek, V. S., and Wefer, G., 139–154, John Wiley and Sons, New York, 1989. 4325

Wong, C. S., Whitney, F. A., Crawford, D. W., Iseki, K., Matear, R. J., Johnson, W. K., Page, J. S., and Timothy, D.: Seasonal and interannual variability in particle fluxes of carbon, nitrogen and silicon from time series of sediment traps at Ocean Station PAPA, 1982–1993: relationship to changes in subarctic primary productivity, Deep-Sea Res. II, 46, 2735–2760, 1999. 4362, 4370

Xu, X., Yamasaki, M., Oda, M., and Honda, M. C.: Comparison of seasonal flux variations of planktonic foraminifera in sediment traps on both sides of the Ryukyu Islands, Japan, Mar. Micropal., 58, 45–55, 2005. 4335, 4362

Žarić, S., Donner, B., Fischer, G., Mulitza, S., and Wefer, G.: Sensitivity of planktic foraminifera to sea surface temperature and export production as derived from sediment trap data, Mar. Micropal., 55, 75–105, 2005. 4325, 4330, 4331, 4335, 4337, 4344, 4362, 4376, 4379, 4382

Žarić, S., Schulz, M., and Mulitza, S.: Global prediction of planktic foraminiferal fluxes from hydrography and productivity data, Biogeosciences, 3, 187–207, 2006, http://www.biogeosciences.net/3/187/2006/. 4326, 4330, 4335

Table 1. Model parameters.

Species	*N. pachyderma* (sin.)	*N. pachyderma* (dex.)	*G.bulloides*	*G.ruber* (white)	*G. sacculifer*
σ	4.0	6.0	6.0	4.0	4.0
T_{opt}(°C)	3.8	15.0	12.0	23.5	28
k	1	1.2^{SP}	1.25^{LP}	1	1
$p(SP)$	0.3	0.2	0.0	0.0	0.0
$p(D)$	0.7	0.8	0.9	0.2	0.1
$p(Z)$	0.0	0.0	0.0	0.6	0.7
$p(DR)$	0.0	0.0	0.1	0.2	0.2
p_2SP	–	0.4	0.2	–	0.0
p_2D	–	0.6	0.8	–	0.3
p_2Z	–	0.0	0.0	–	0.6
p_2DR	–	0.0	0.0	–	0.1
$G_{max}(SP, D, DR)$	1.08	1.08	1.08	1.08	1.08
$G_{max}(Z)$	2.16	2.16	2.16	2.16	2.16
g	0.66	0.66	0.66	0.66	0.66
d	–	0.05	0.5	1	1
$cl_{N.\ pachyderma(sin.)}$	–	0.2	0	0	0
$cl_{N.\ pachyderma(dex.)}$	–	–	0	1	0
$cl_{G.\ bulloides}$	–	0	–	1	1
$cl_{G.\ ruber(white)}$	–	0	0.5	–	0.8
$cl_{G.\ sacculifer}$	–	0	0.5	0.8	–
pl	1	4	5	5	4
rl	0.06	0.06	0.06	0.06	0.06
b	4000	4000	4000	4000	4000
Z_{ingest}	0.3	0.3	0.3	0.3	0.3

σ = standard deviation of optimal temperature
T_{opt} = optimal temperature (°C)
k = parameter to control temperature tolerance range depending on the food availability
$p(SP)$ = preference for grazing on small phytoplankton
$p(D)$ = preference for grazing on diatoms
$p(Z)$ = preference for grazing on zooplankton
$p(DR)$ = preference for grazing on detritus
$G_{max}(SP)$ = maximum growth rate when grazing on small phytoplankton (per day)
$G_{max}(D)$ = maximum growth rate when grazing on diatoms (per day)
$G_{max}(Z)$ = maximum growth rate when grazing on zooplankton (per day)
$G_{max}(DR)$ = maximum growth rate when grazing on detritus (per day)
g = half-saturation constant for grazing
GGE = portion of grazed matter that is incorporated into foraminifera biomass (Gross Growth Efficiency)
pl = quadratic mortality rate coefficient
rl = respiration loss (per day)
cl_{ij} = effect of competition of the species i upon the species j
C = food type (SP, D, Z or DR)
SP = small phytoplankton [mmolC/m^3]
D = diatoms [mmolC/m^3]
Z = zooplankton [mmolC/m^3]
DR = detritus [mmolC/m^3]

Table 2. Locations, trap and water depths, sieve size and data sources of the planktonic foraminifera faunas.

Trap Location	Latitude[° N]	Longitude[° E]	Trap depth [m]	Water depth [m]	Sieve size [μm]	References
Ocean Station Papa	50.00	−145.00	3800	4240	≥125	Reynolds and Thunell (1985) Sautter and Thunell (1989) Wong et al. (1999)
Peru-Chile Current	−30.01	−73.18	2318	4345	≥150	Marchant et al. (1998) Hebbeln et al. (2000)
N' North Atlantic	72.38 69.69	−7.71 0.48	500; 1000; 2300 500; 1000	2624 3254	≥125 ≥125	Jensen (1998) Peinert et al. (2001)
Cape Blanc	20.76 21.15	−19.74 −20.68	2195 732; 3552	3646 4103	≥150 ≥150	Fischer and Wefer (1996) Fischer et al. (1996) Žarić et al. (2005)
W' equatorial Atlantic	−4.00 −7.52	−25.57 −28.04	652; 1232; 4991 631; 5031	5330 5570	≥150 ≥150	Fischer and Wefer (1996) Fischer (unpubl. data); Žarić et al. (2005)
W Atlantic	−11.57	−28.53	719; 4515	5472	≥150	Fischer (unpubl. data) Žarić et al. (2005)
E' equatorial Atlantic	3.17 1.78 −0.08 −2.19	−11.25 −11.25 −10.77 −10.09	984 953 1097 1068	4524 4399 4141 3906	≥150 ≥150 ≥150 ≥150	Fischer and Wefer (1996) Žarić et al. (2005)
Walvis Ridge	−20.05 −20.13	9.16 8.96	599; 1648 1717	2202 2263	≥150 ≥150	Fischer and Wefer (1996) Žarić et al. (2005)
Wedell Sea	−62.44 −64.91	−34.76 −2.55	868 352; 4456	3880 5032	≥125 ≥125	Donner and Wefer (1994)
Arabian Sea	16.33 14.49 15.48 24.65	60.49 64.76 68.74 65.81	1028; 3026 733; 2909 1401; 2775 590	4016 3901 3774 1166	≥150 ≥150 ≥125 ≥125	Curry et al. (1992) Guptha and Mohan (1996) Haake et al. (1993) Schulz et al. (2002)
Bay of Bengal	17.45 13.15	89.60 84.35	967; 1498; 2029 950; 2286	2263 3259	≥150 ≥150	Guptha and Mohan (1996) Guptha et al. (1997)
Northwest Pacific	25.00 39.01	136.99 147.00	917; 1388; 4336; 4758 1371; 1586; 4787	5107 5339	≥125 ≥125	Mohiuddin et al. (2002)
NW' North Pacific	50.02 43.97 40.00	165.03 155.05 165.00	3260 2957 2986	5570 5370 5483	≥125 ≥125 ≥125	Kuroyanagi et al. (2002)
Subantartic Zone	−46.76 −51.00 −53.75	142.07 141.74 141.76	1060; 3850 3080 830; 1580	4540 3780 2280	≥150 ≥150 ≥150	King and Howard (2003a,b) Trull et al. (2001)
Chatman Rise	−42.70 −44.62	178.63 178.62	300; 1000 300; 1000	1500 1500	≥150 ≥150	King and Howard (2003a,b) Nodder and Northcote (2001)
Cariaco Basin	10.50	−64.67	275	1400	≥125	Tedesco and Thunell (2003)
Japan Trench	34.16 34.17	141.98 141.97	1174; 3680 1174; 3700	8942 8941	≥125 ≥125	Oda and Yamasaki (2005)
Ryukyu Islands	27.38 25.07	126.73 127.58	1000 3000	1627 3771	≥125 ≥125	Xu et al. (2005)
Bering Sea	53.53 49.00	−177.00 −174.00	3198 4812	3788 5406	≥125 ≥125	Asahi and Takahashi (2007)
South China Sea	14.60	115.11	1208	4270	≥125	Tian et al. (2005)

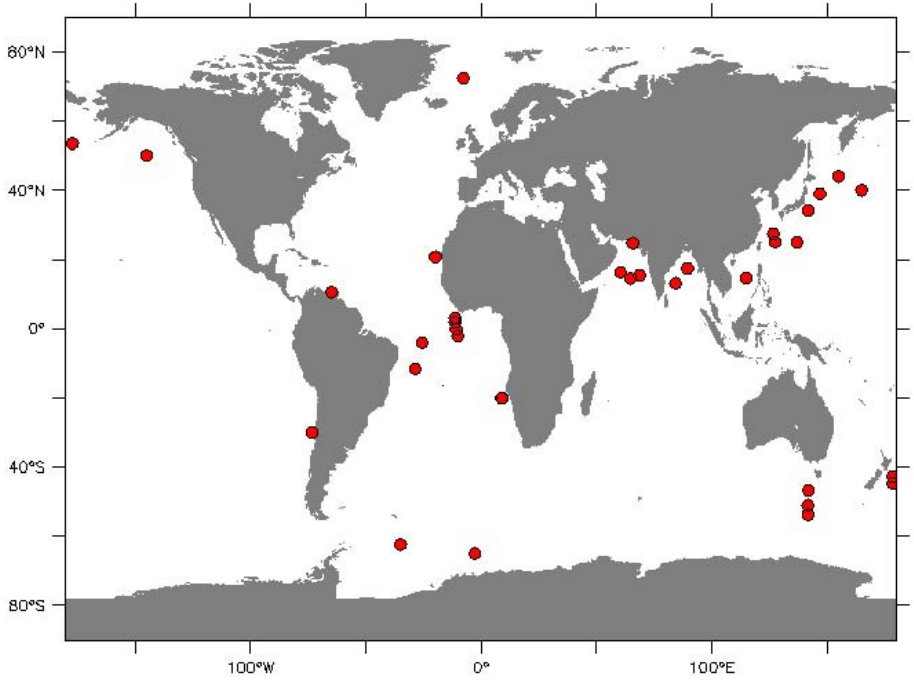

Fig. 1. Locations of the sediment-trap stations used to compare measured and modeled foraminiferal fluxes. Details of the trap depth, sieve size and references in Table 2.

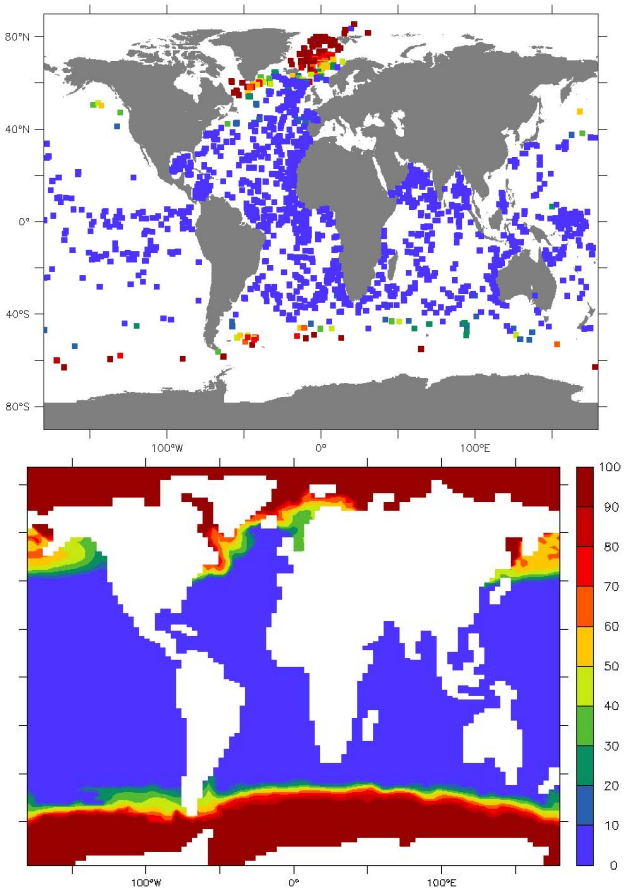

Fig. 2. *N. pachyderma* (sin.) relative abundances from core-top (left) foraminiferal assemblages (Prell et al., 1999; Martinez et al., 1998; Pflauman et al., 1996) and PLAFOM (right). Relative abundances consider only the species included in the model. RMSE is 10%.

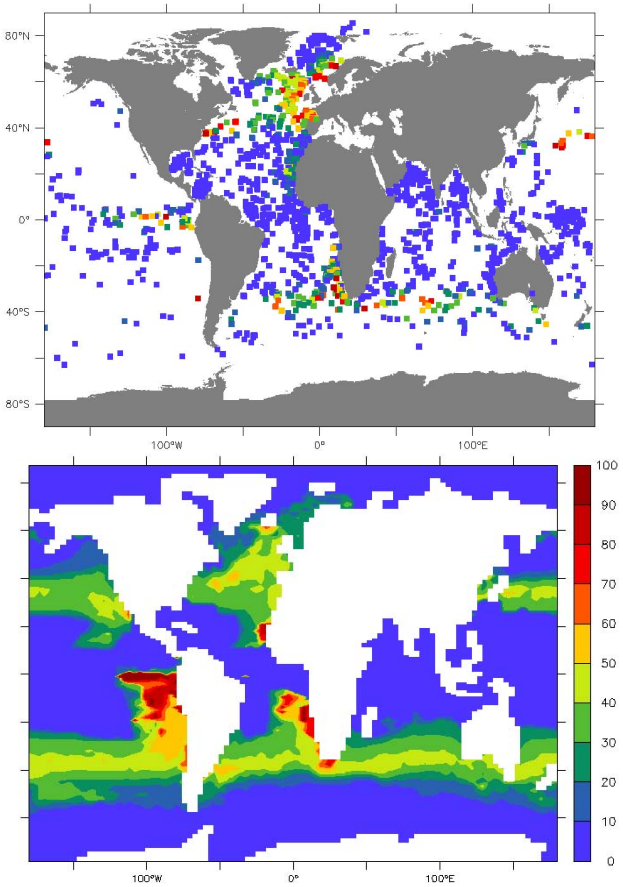

Fig. 3. *N. pachyderma* (dex.) relative abundances from core-top (left) foraminiferal assemblages (Prell et al., 1999; Marchant et al., 1998; Pflauman et al., 1996) and PLAFOM (right). Relative abundances consider only the species included in the model. RMSE is 21%.

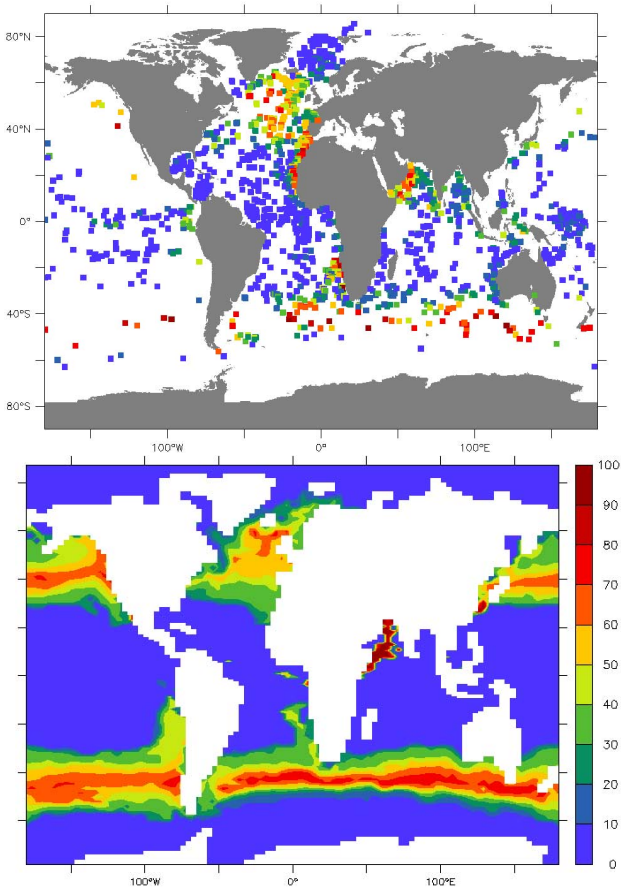

Fig. 4. *G. bulloides* relative abundances from core-top (left) foraminiferal assemblages (Prell et al., 1999; Marchant et al., 1998; Pflauman et al., 1996) and PLAFOM (right). Relative abundances consider only the species included in the model. RMSE is 24%.

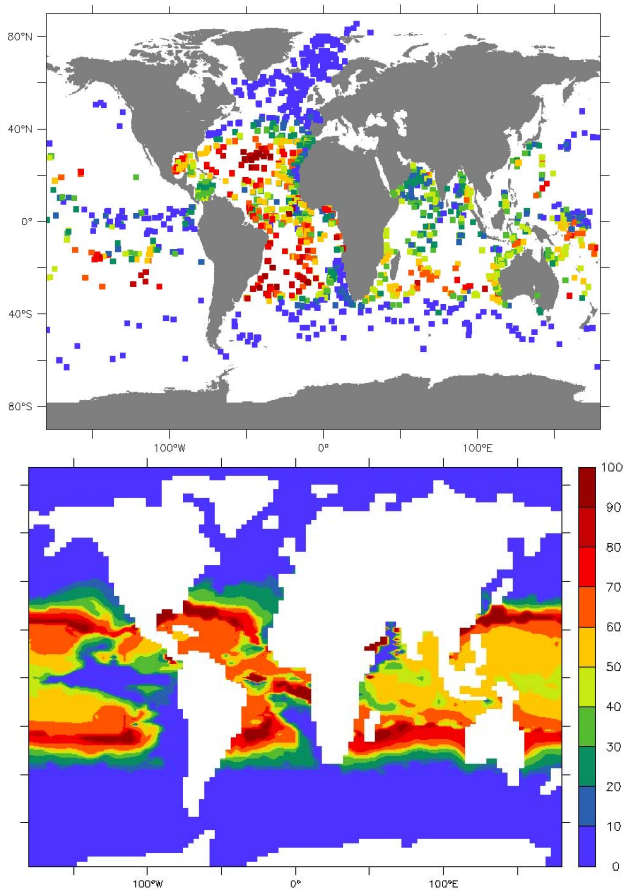

Fig. 5. *G. ruber* (white) relative abundances from core-top (left) foraminiferal assemblages (Prell et al., 1999; Marchant et al., 1998; Pflauman et al., 1996) and PLAFOM (right). Relative abundances consider only the species included in the model. RMSE is 25%.

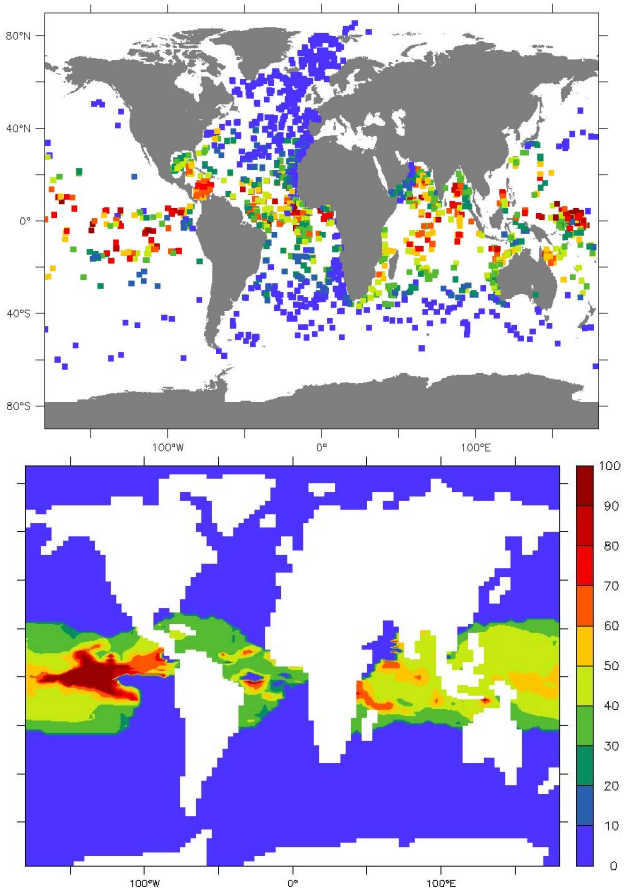

Fig. 6. *G. sacculifer* relative abundances from core-top (left) foraminiferal assemblages (Prell et al., 1999; Martinez et al., 1998; Pflauman et al., 1996) and PLAFOM (right). Relative abundances consider only the species included in the model. RMSE is 23%.

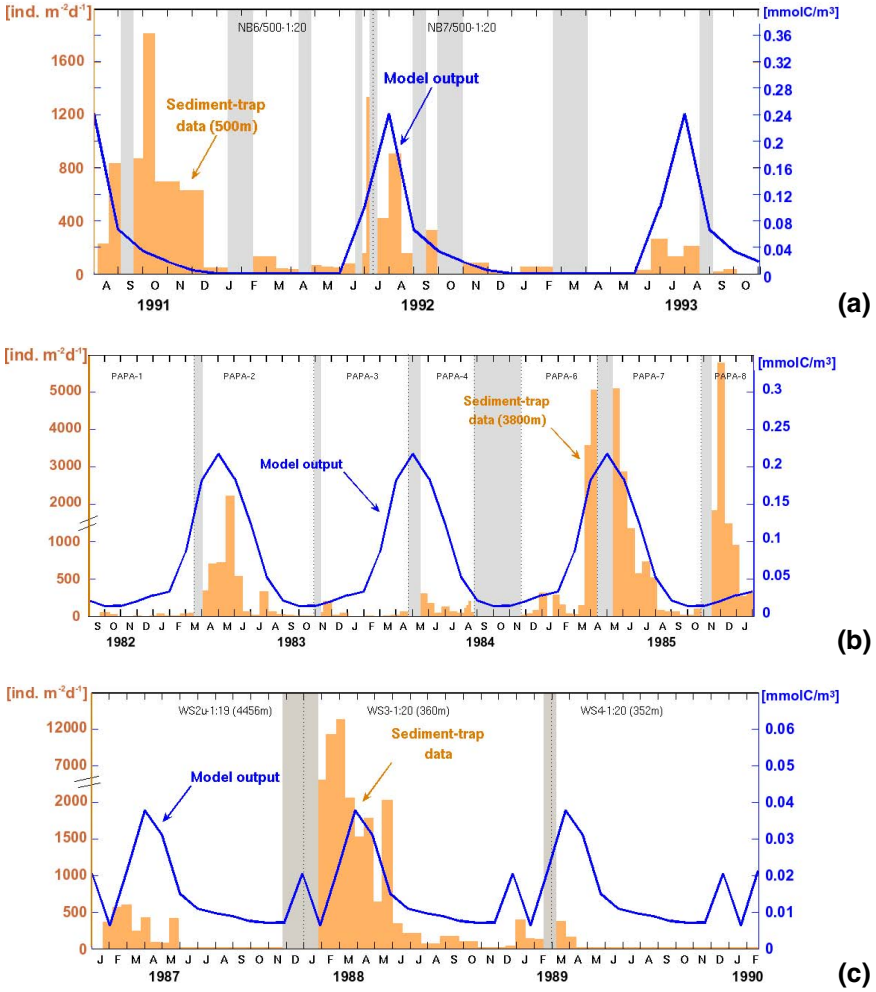

Fig. 7.

BGD
4, 4323–4384, 2007

EGU

Fig. 7. Comparison of measured foraminiferal fluxes of *N. pachyderma* (sin.) in sediment-traps (orange bars) vs. modeled abundances (blue lines). Note the difference in units from sediment-traps [ind. m^{-2} day^{-1}] to the model output [mmolC/m^3]. The shadow represent period of time when for technical reasons the trap could not get any data. **(a)** northern North Atlantic, 69.69° N 0.48° E (Jensen, 1998); **(b)** Ocean Station PAPA, in Northwest Pacific, 50.00° N 145.00° W (Reynolds and Thunell, 1985; Sautter and Thunell, 1989; Wong et al., 1999); **(c)** Wedell Sea, 64.91° S 2.55° W, in the Southern Ocean (Donner and Wefer, 1994).

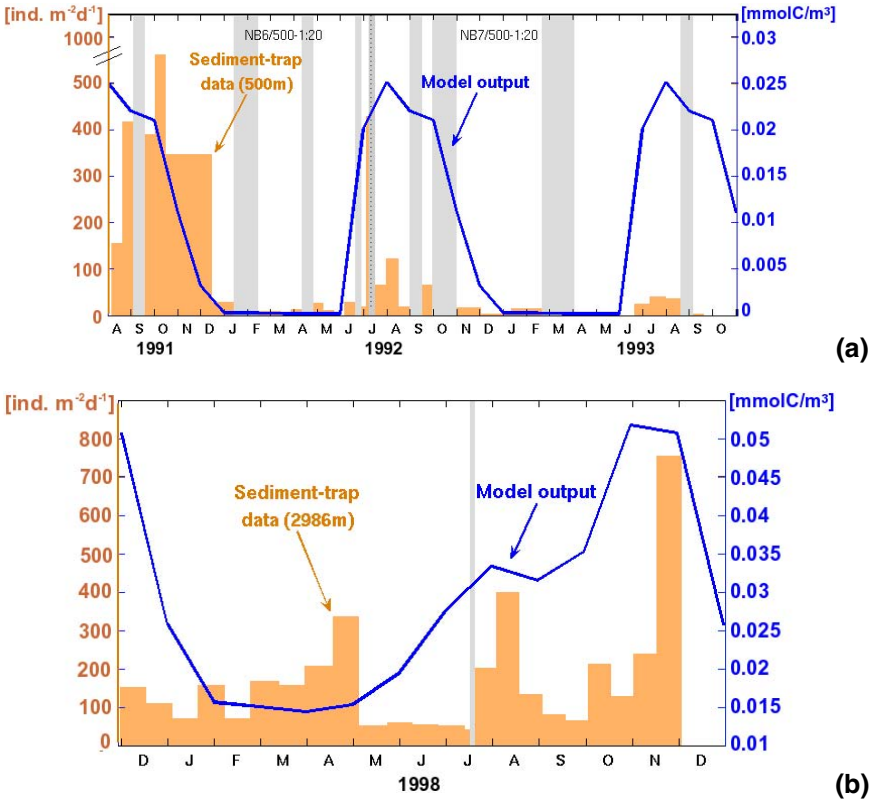
[ind. m-2d-1]
[mmolC/m3]
NB6/500-1:20
NB7/500-1:20
Sediment-trap data (500m)
Model output
1000
500
400
300
200
100
0
0.03
0.025
0.02
0.015
0.01
0.005
0
A S O N D J F M A M J J A S O N D J F M A M J J A S O
1991
1992
1993
(a)
[ind. m-2d-1]
[mmolC/m3]
Sediment-trap data (2986m)
Model output
800
700
600
500
400
300
200
100
0
0.05
0.045
0.04
0.035
0.03
0.025
0.02
0.015
0.01
D J F M A M J J A S O N D
1998
(b)

Fig. 8.

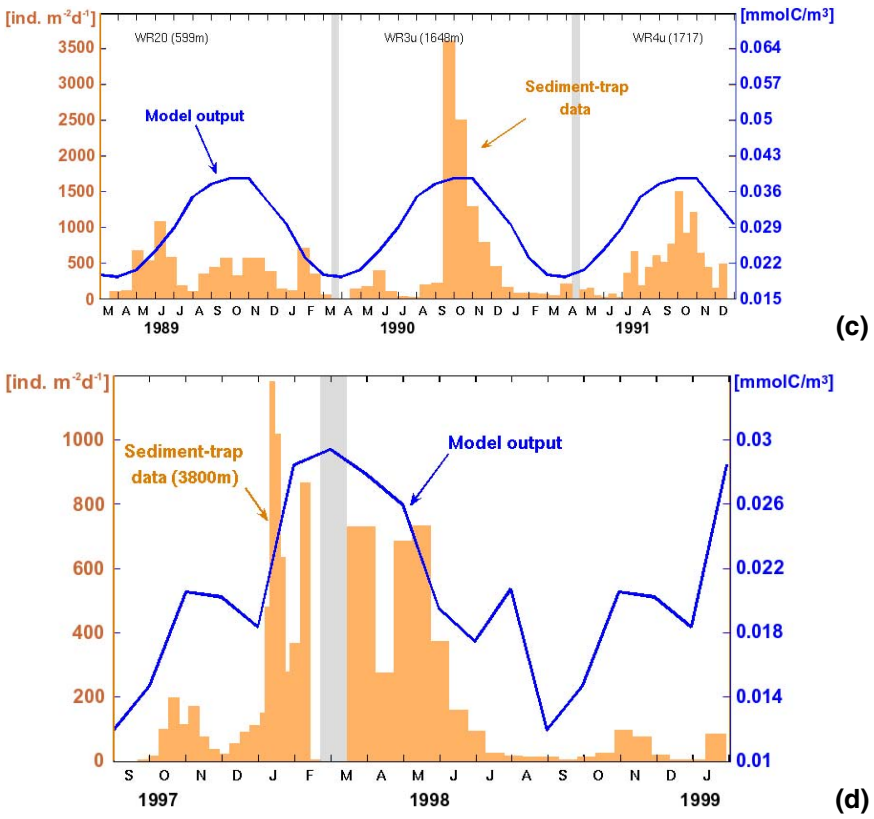
[ind. m-2d-1]
[mmolC/m3]
WR2O (599m)
WR3u (1648m)
WR4u (1717)
Model output
Sediment-trap data
3500
3000
2500
2000
1500
1000
500
0
0.064
0.057
0.05
0.043
0.036
0.029
0.022
0.015
M A M J J A S O N D J F M A M J J A S O N D J F M A M J J A S O N D
1989
1990
1991
(c)
[ind. m-2d-1]
[mmolC/m3]
Sediment-trap data (3800m)
Model output
1000
800
600
400
200
0
0.03
0.026
0.022
0.018
0.014
0.01
S O N D J F M A M J J A S O N D J
1997
1998
1999
(d)

Fig. 8.

Fig. 8. Comparison of measured foraminiferal fluxes of *N. pachyderma* (dex.) in sediment-traps (orange bars) vs. modeled abundances (blue lines). Note the difference in units from sediment-traps [ind. m^{-2} day^{-1}] to the model output [mmolC/m^3]. The shadow represent period of time when for technical reasons the trap could not get any data. **(a)** northern North Atlantic, 69.69° N 0.48° E (Jensen, 1998); **(b)** northwestern North Pacific, 40.00° N 165.00° E (Kuroyanagi et al., 2002); **(c)** Walvis Ridge in South Atlantic, 20.05° S 9.16° E (Fischer and Wefer, 1996); **(d)** Subantartic Zone, 46.76° S 142.07° E (King and Howard, 2003a,b; Trull et al., 2001).

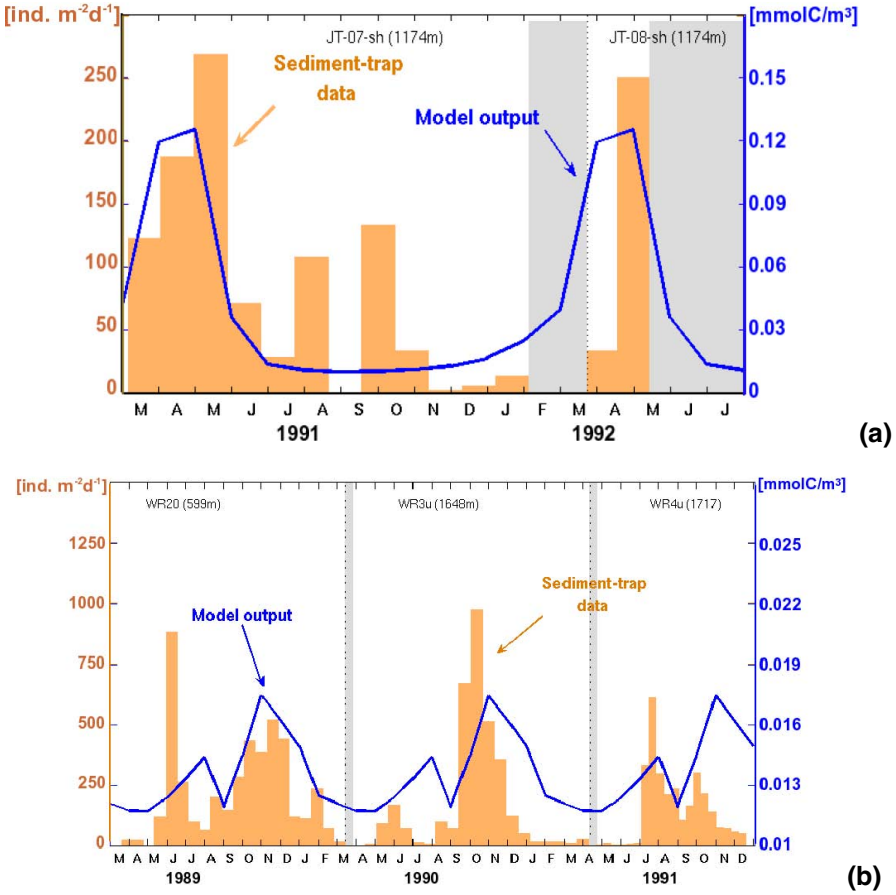
[ind. m-2d-1]
[mmolC/m3]
JT-07-sh (1174m)
JT-08-sh (1174m)
Sediment-trap data
Model output
250
200
150
100
50
0
0.15
0.12
0.09
0.06
0.03
0
M A M J J A S O N D J F M A M J J
1991
1992
(a)
[ind. m-2d-1]
[mmolC/m3]
WR2O (599m)
WR3u (1648m)
WR4u (1717)
Model output
Sediment-trap data
1250
1000
750
500
250
0
0.025
0.022
0.019
0.016
0.013
0.01
M A M J J A S O N D J F M A M J J A S O N D J F M A M J J A S O N D
1989
1990
1991
(b)

Fig. 9.

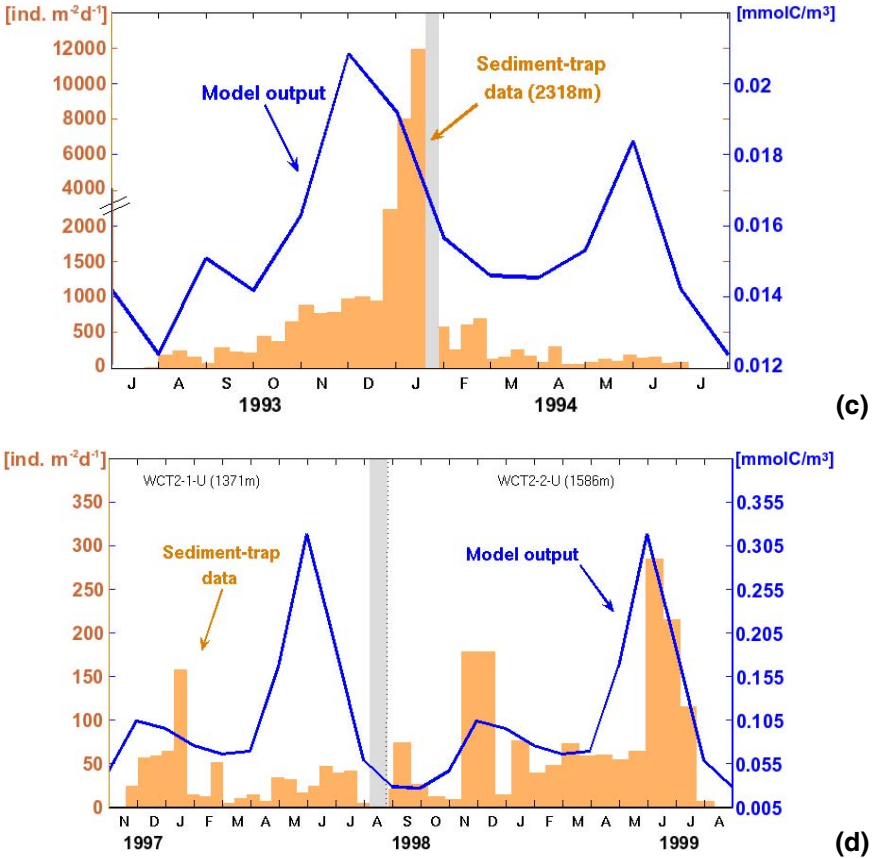
[ind. m-2d-1]
[mmolC/m3]
Model output
Sediment-trap data (2318m)
12000
10000
8000
6000
4000
2000
1500
1000
500
0
0.02
0.018
0.016
0.014
0.012
J A S O N D J F M A M J J
1993
1994
(c)
[ind. m-2d-1]
[mmolC/m3]
WCT2-1-U (1371m)
WCT2-2-U (1586m)
Sediment-trap data
Model output
350
300
250
200
150
100
50
0
0.355
0.305
0.255
0.205
0.155
0.105
0.055
0.005
N D J F M A M J J A S O N D J F M A M J J A
1997
1998
1999
(d)

Fig. 9.

Fig. 9. Comparison of measured foraminiferal fluxes of *G. bulloides* in sediment-traps (orange bars) vs. modeled abundances (blue lines). Note the difference in units from sediment-traps [ind. m^{-2} day^{-1}] to the model output [mmolC/m^3]. The shadow represent period of time when for technical reasons the trap could not get any data. **(a)** Japan Trench, 34.16° N 141.98° E (Oda and Yamasaki, 2005); **(b)** Walvis Ridge, 20.05° S 9.16° E (Fischer and Wefer, 1996; Žarić et al., 2005); **(c)** Peru-Chile current, 30.01° S 73.18° W (Marchant et al., 1998; Hebbeln et al., 2000); **(d)** Northwest Pacific, 39.01° N 147.00° E (Mohiuddin et al., 2002).

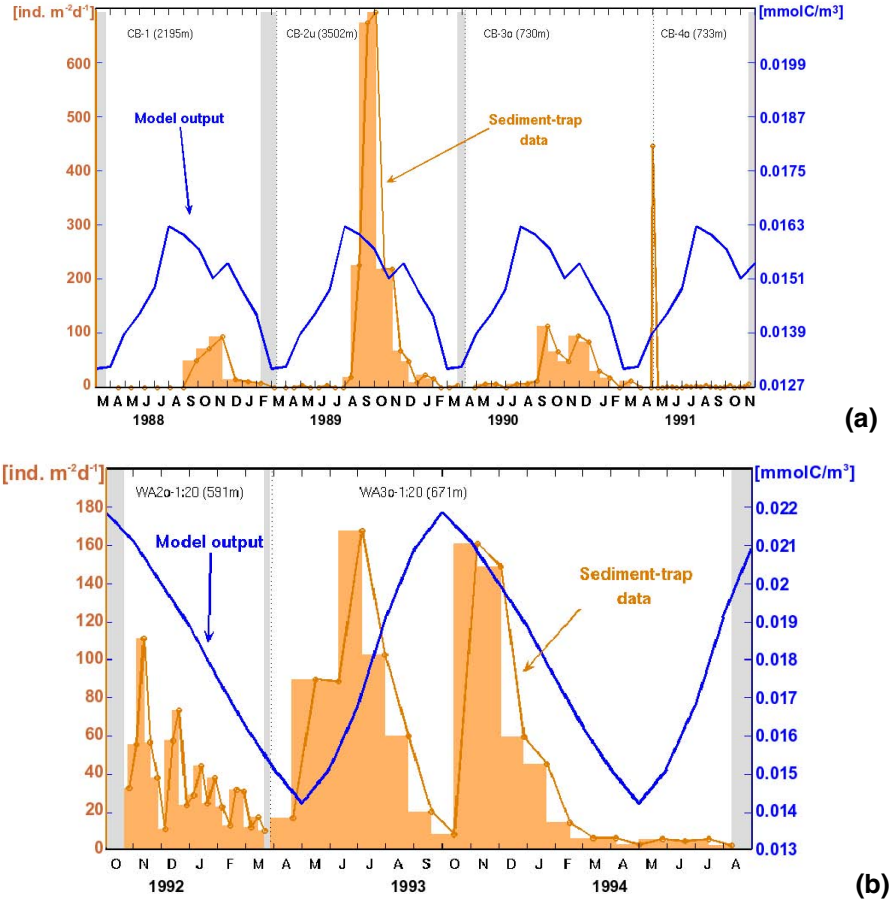
[ind. m-2d-1]
[mmolC/m3]
CB-1 (2195m)
CB-2u (3502m)
CB-3o (730m)
CB-4o (733m)
Model output
Sediment-trap data
600
500
400
300
200
100
0
0.0199
0.0187
0.0175
0.0163
0.0151
0.0139
0.0127
M A M J J A S O N D J F M A M J J A S O N D J F M A M J J A S O N D J F M A M J J A S O N
1988
1989
1990
1991
(a)
[ind. m-2d-1]
[mmolC/m3]
WA2o-1:20 (591m)
WA3o-1:20 (671m)
Model output
Sediment-trap data
180
160
140
120
100
80
60
40
20
0
0.022
0.021
0.02
0.019
0.018
0.017
0.016
0.015
0.014
0.013
O N D J F M A M J J A S O N D J F M A M J J A
1992
1993
1994
(b)

Fig. 10.

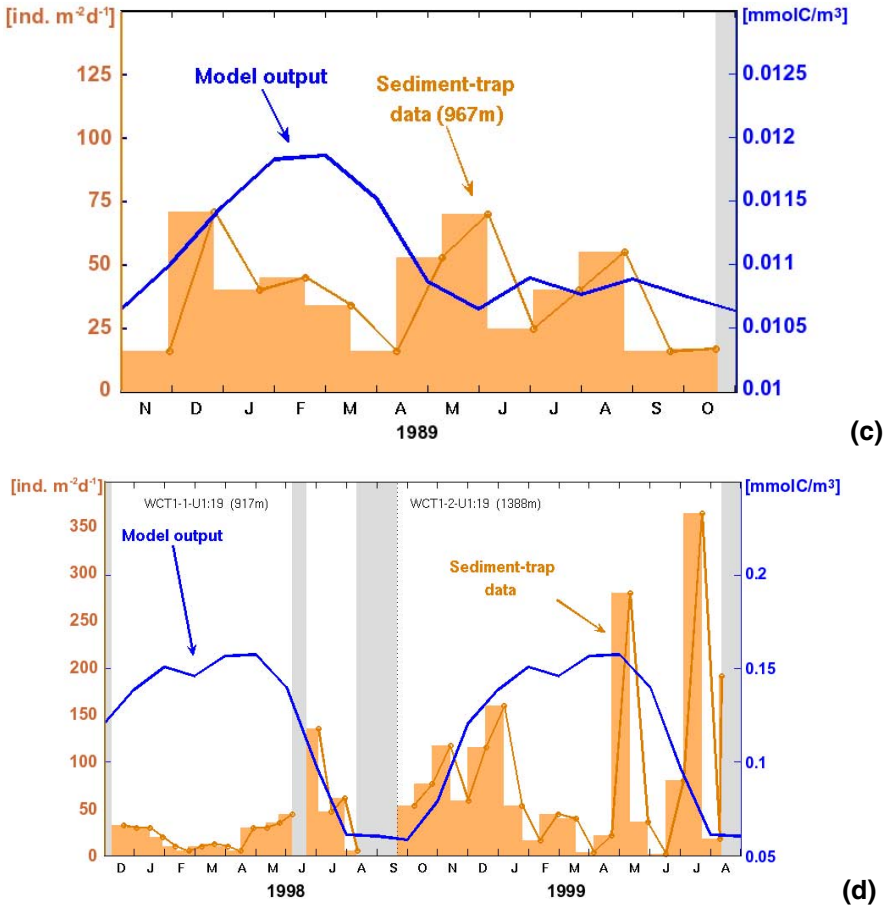
[ind. m-2d-1]
[mmolC/m3]
Model output
Sediment-trap data (967m)
125
100
75
50
25
0
0.0125
0.012
0.0115
0.011
0.0105
0.01
N D J F M A M J J A S O
1989
(c)
[ind. m-2d-1]
[mmolC/m3]
WCT1-1-U1:19 (917m)
WCT1-2-U1:19 (1388m)
Model output
Sediment-trap data
350
300
250
200
150
100
50
0
0.2
0.15
0.1
0.05
D J F M A M J J A S O N D J F M A M J J A
1998
1999
(d)

Fig. 10.

Fig. 10. Comparison of measured foraminiferal fluxes of *G. ruber* (white) in sediment-traps (orange bars) vs. modeled abundances (blue lines). Note the difference in units from sediment-traps [ind. m^{-2} day^{-1}] to the model output [mmolC/m^3]. The shadow represent period of time when for technical reasons the trap could not get any data. **(a)** Cape Blanc, 21.15° N 20.69° W (Fischer and Wefer, 1996; Fischer et al., 1996; Žarić et al., 2005); **(b)** western equatorial Atlantic, 7.51° S 28.03° W (Fischer and Wefer, 1996; Fischer et al., 1996; Žarić et al., 2005); **(c)** Bay of Bengal, 17.45° N 89.60° E (Guptha and Mohan, 1996; Guptha et al., 1997); **(d)** Northwest Pacific, 25.00° N 136.99° E (Mohiuddin et al., 2002).

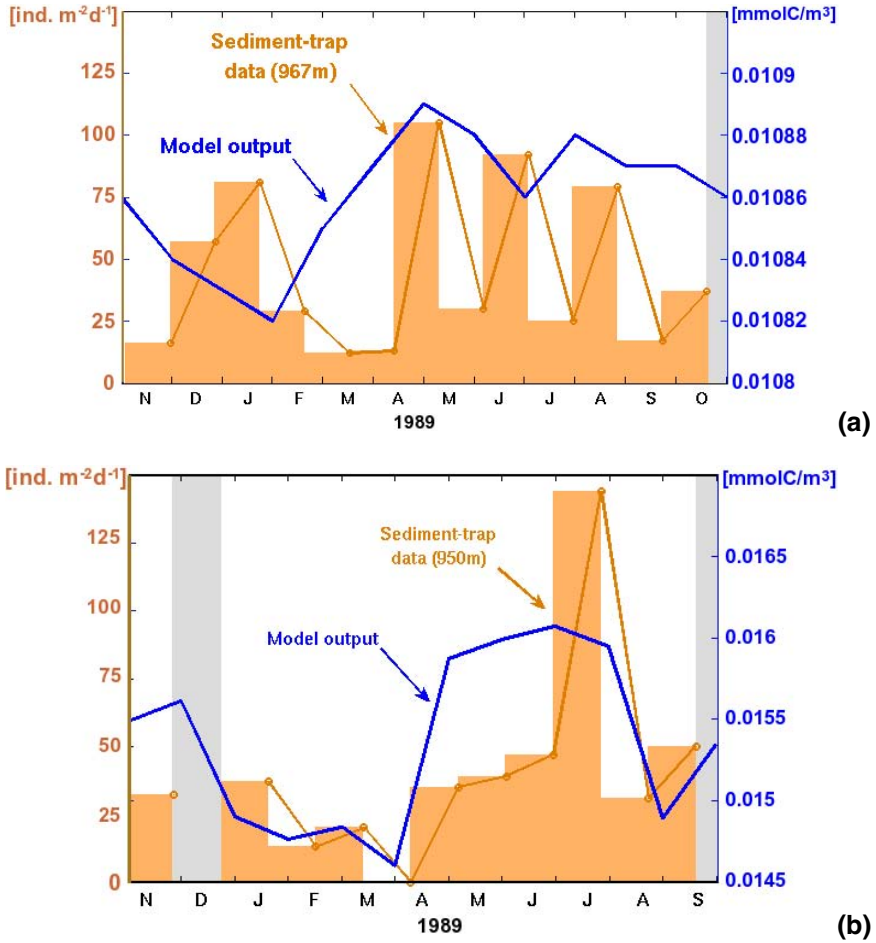
[ind. m-2d-1]
[mmolC/m3]
Sediment-trap data (967m)
Model output
125
100
75
50
25
0
0.0109
0.01088
0.01086
0.01084
0.01082
0.0108
N D J F M A M J J A S O
1989
(a)
[ind. m-2d-1]
[mmolC/m3]
Sediment-trap data (950m)
Model output
125
100
75
50
25
0
0.0165
0.016
0.0155
0.015
0.0145
N D J F M A M J J A S
1989
(b)

Fig. 11.

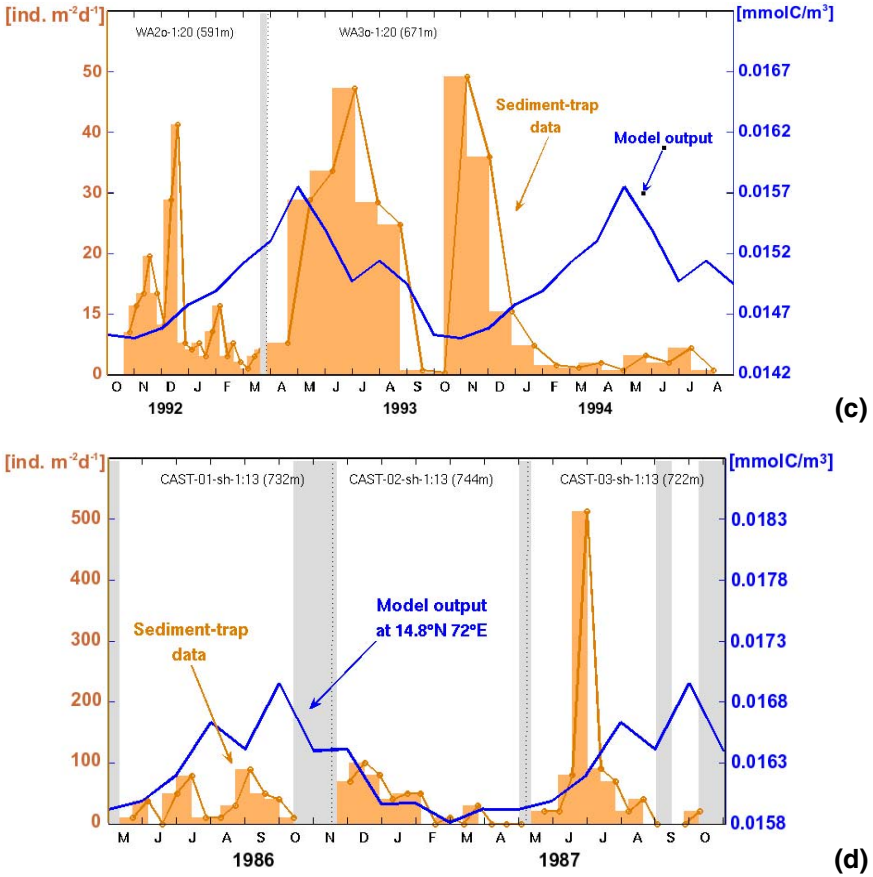
[ind. m-2d-1]
[mmolC/m3]
WA2o-1:20 (591m)
WA3o-1:20 (671m)
Sediment-trap data
Model output
50
40
30
20
15
0
0.0167
0.0162
0.0157
0.0152
0.0147
0.0142
O N D J F M A M J J A S O N D J F M A M J J A
1992
1993
1994
(c)
[ind. m-2d-1]
[mmolC/m3]
CAST-01-sh-1:13 (732m)
CAST-02-sh-1:13 (744m)
CAST-03-sh-1:13 (722m)
Sediment-trap data
Model output at 14.8°N 72°E
500
400
300
200
100
0
0.0183
0.0178
0.0173
0.0168
0.0163
0.0158
M J J A S O N D J F M A M J J A S O
1986
1987
(d)

Fig. 11.

Fig. 11. Comparison of measured foraminiferal fluxes of *G. sacculifer* in sediment-traps (orange bars) vs. modeled abundances (blue lines). Note the difference in units from sediment-traps [ind. m^{-2} day^{-1}] to the model output [mmolC/m^3]. The shadow represent period of time when for technical reasons the trap could not get any data. **(a)** northern Bay of Bengal, 17.45° N 89.60° E (Guptha and Mohan, 1996; Guptha et al., 1997) **(b)** central Bay of Bengal, 13.15° N 89.35° E (Guptha and Mohan, 1996; Guptha et al., 1997); **(c)** western equatorial Atlantic, 7.52° S 28.04° W (Fischer and Wefer, 1996; Fischer et al., 1996; Žarić et al., 2005); **(d)** Arabian Sea, 14.49° N 65.76° E (Curry et al., 1992; Haake et al., 1993).

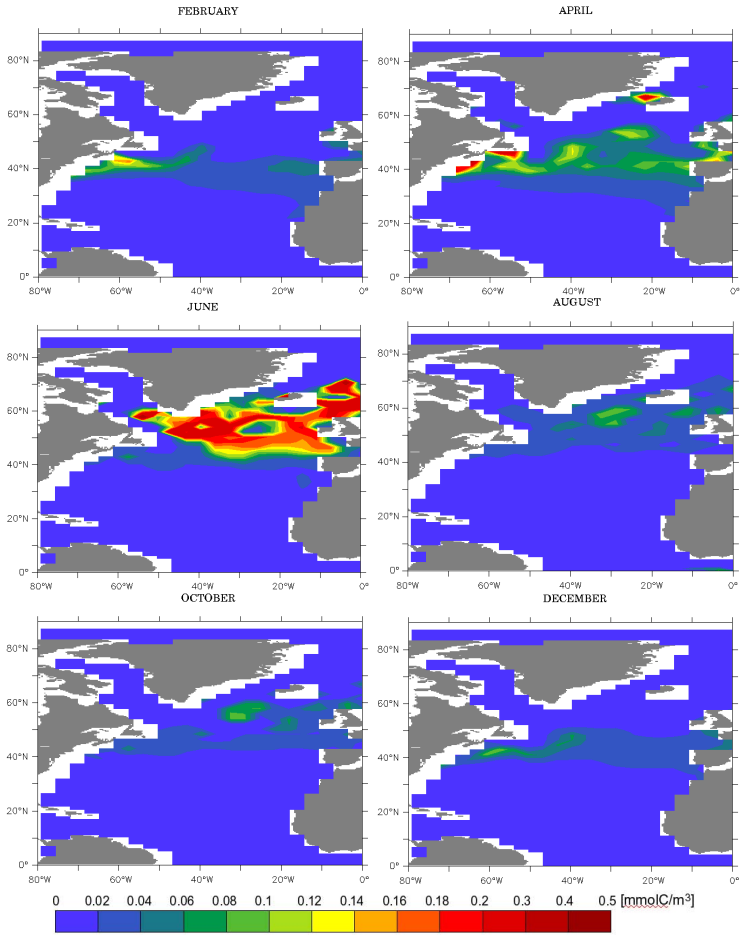

Fig. 12. PLAFOM-standard run. Modeled monthly concentrations of *G. bulloides* in the North Atlantic during the simulation year. Units given in mmolC/m^3.

BGD
4, 4323–4384, 2007

EGU

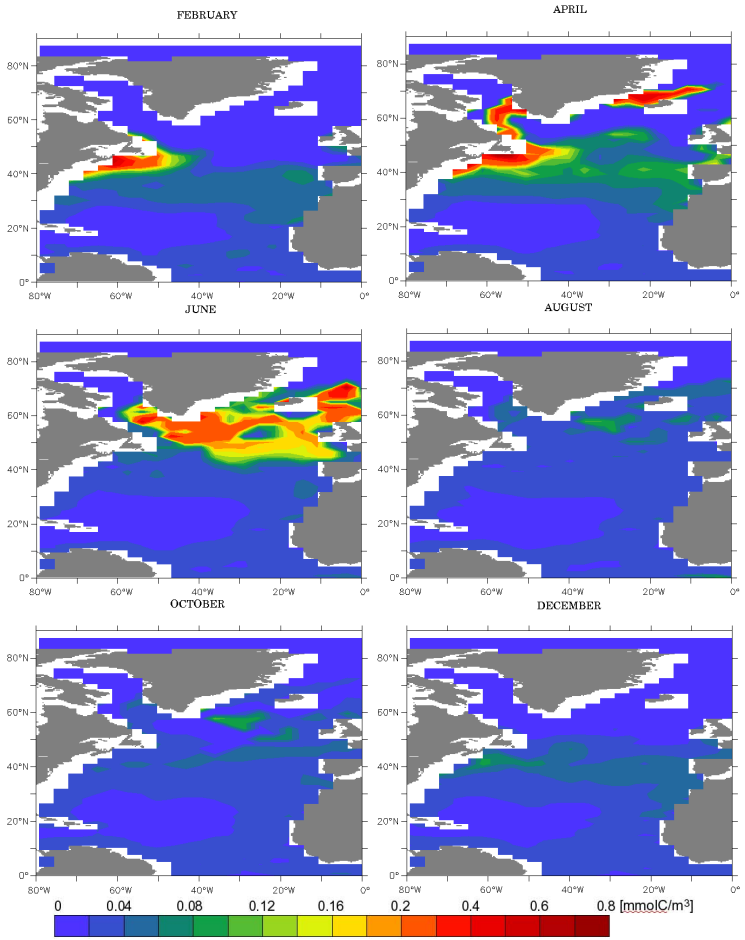

Fig. 13. PLAFOM-experiment with constant mixed layer temperature of 12 °C. Modeled monthly concentrations of *G. bulloides* in the North Atlantic during the experimental simulation. Units given in mmolC/m^3.